Electronic Supplementary Material (ESI) for Chemical Science.

Supporting Information

Unmasking the Constitution and Bonding of the Proposed Lithium Nickelate "$Li_3NiPh_3(solv)_3$": Revealing the hidden C_6H_4 ligand

Rosie J. Somerville, Andryj M. Borys, Marina Perez-Jimenez, Ainara Nova, David Balcells, Lorraine A. Malaspina, Simon Grabowsky, Ernesto Carmona, Eva Hevia,* Jesús Campos*

E-mail: jesus.campos@iiq.csic.es, eva.hevia@unibe.ch

Table of Contents

General Considerations 3

Preparation of Ni complexes 4

$[Li_2(Et_2O)_4(LiBr)Ph_2Ni]_2COD$ (**4**) 4

$[Li_2(THF)_4NiPh_4]$ 4

$Li_6(Et_2O)_4Ph_6Ni_2(C_6H_4)$ (**5**) 5

$Li_5(THF)_5Ph_5Ni_2(C_6H_4)$ (**6**) 6

$[Li_2(THF)_4NiPh_4]$ + PhLi 7

PhNa 8

$[Na_2(solv)_3Ph_2Ni(olefin)]_2$ (**7**) 8

$[Na_2(Et_2O)_3Ph_2(NaC_8H_{11})NiCOD]_2$ (**8**) 9

NMR Studies 10

DOSY NMR Studies on **5** 10

NOE and EXSY NMR Studies on **5** 11

Variable Temperature NMR Studies on **5** and **6** 12

LiH Trapping Reactions 18

Attempted Trapping with BH_3 18

Attempted Trapping with Benzophenone 19

Stoichiometric reactivity of **5** and **6** 20

Experiments with PhLi-$^{13}C_6$ 23

Catalysis 25

Reactivity of intermediate nickelates with N_2 26

X-ray Crystallography 27

Complexes **4**, **5**, and N_2-Complex 27

Complexes **6**, **7**, and **8** 27

Molecular Structure of **4** 30

Molecular Structure of **5** 31

Molecular Structure of N_2-Complex 32

Molecular Structure of **6** 33

Molecular Structure of **7** 34

Molecular Structure of **8** 35

NMR Spectra of Reported Compounds 36

Computational Details 43

References 46

General Considerations

All manipulations were carried out under an inert atmosphere of argon using standard Schlenk line or glovebox techniques (MBraun UNILab Pro ECO, <0.1 ppm H_2O and O_2). Due to the extreme air, moisture, and temperature sensitivity of described compounds, rigorously inert conditions must be maintained to allow for the isolation of crystalline and spectroscopically pure samples. Glass-coated stir bars are preferable for reactions involving PhLi, PhNa and nickelate complexes. Specific experimental details can be found below.

THF was dried and distilled from Na/benzophenone and stored over 4 Å molecular sieves, then further dried and vacuum distilled over a sodium mirror. Hexane, pentane, Et_2O, toluene and benzene were pre-dried using a MBraun MBSPS 5, then further dried and vacuum distilled over $NaK_{2.8}$ or a sodium mirror, and stored over 4 Å molecular sieves.THF-d_8, toluene-d_8 and C_6D_6 were dried and distilled over $NaK_{2.8}$ and stored over 4 Å molecular sieves in a glovebox prior to use. $Ni(COD)_2$ was purchased from Sigma Aldrich or Strem Chemicals. $Ni(\eta^5\text{-}C_5H_5)_2$ was purchased from Sigma Aldrich.

$[PhLi]_\infty$ and $[PhLi(THF)]_4$ were prepared as previously reported.[1,2] The syntheses of $[(PhLi{\cdot}Et_2O)_3{\cdot}LiBr]$ and $[(PhLi{\cdot}Et_2O)_3{\cdot}LiBr]$-$^{13}C_6$ were carried out by combining equimolar amounts of the appropriate PhBr and *t*-BuLi in Et_2O at −78 °C.[3] Compound **2** was prepared according to literature procedures.[1]

NMR spectra were recorded on Bruker Avance III HD 300 or 400 MHz spectrometers at 300 K unless otherwise specified. ^{1}H NMR spectra were referenced internally to the corresponding residual *protio* solvent peaks. ^{7}Li was referenced to LiCl. CHN elemental microanalyses were performed on a Flash 2000 Organic Elemental Analyser (Thermo Scientific) or a LECO TruSpec CHN analyser.

Preparation of Ni complexes

We did not examine the pyrophoricity of the novel alkali-metal nickelates in detail. Handling of solid PhLi and PhNa (and solid Ni complexes containing excess of either) should be carried out with care due to the pyrophoricity of these solids.

$[Li_2(Et_2O)_4(LiBr)Ph_2Ni]_2COD$ (4)

$Ni(COD)_2$ (43.9 mg, 0.16 mmol, 1 equiv) and $[(PhLi{\cdot}OEt_2)_3{\cdot}LiBr]$ (75.9 mg, 0.14 mmol, 0.88 equiv) were weighed into a vial containing a stir bar. Pentane (3 mL) was added and the solids stirred together vigorously for 1 hour. The light orange pentane solution was decanted from the tan solid, then the solid suspended in 5 mL pentane, filtered, and washed with pentane (5 × 1.5 mL). After drying under vacuum, **4** was obtained as a tan-orange solid. Yield = 76.6 mg (37%).

Recrystallisation to form large orange blocks was achieved by adding pentane (0.5 mL) followed by Et_2O until the solid was dissolved, then cooling the resulting red solution to −35 ºC for a week.

^{1}H NMR (400 MHz, THF-d_8, 25 °C): δ 7.90 (d, 8 H, $^3J_{H\text{-}H}$ = 7.06 Hz, PhNi-*o*-C*H*), 6.70 (t, 8 H, $^3J_{H\text{-}H}$ = 7.19 Hz, PhNi-*m*-C*H*), 6.50 (m, 4 H, PhNi-*p*-C*H*), 3.15 (br s, Δv1/2 = 25 Hz, 4 H, COD-C*H*), 1.95 (s, 8 H, COD-CH_2).

^{13}C{^{1}H} NMR (100 MHz, THF-d_8, 50 °C): δ 191.5 (PhNi-*ipso*-*C*), 142.0 (PhNi-*o*-*C*), 125.4 (PhNi-*m*-*C*), 119.0 (PhNi-*p*-*C*), 86.4 (br, $\Delta v_{1/2}$ = 190 Hz, COD-*C*H), 32.5 (COD-*C*H_2).

^{7}Li{^{1}H} NMR (161 MHz, THF-d_8, 25 °C): δ 0.32 (s).
^{7}Li{^{1}H} NMR (161 MHz, THF-d_8, −70 °C): δ 0.61 (s), 0.15 (s) (2:1 ratio).

Elemental analysis: Calc. for $C_{64}H_{96}Br_2Li_6Ni_2O_8$: C, 58.58; H, 7.37; Found: C, 58.69; H, 7.39 (for the THF solvate).

$[Li_2(THF)_4NiPh_4]$

A synthetic route using a commercially available Ni(II) precursor was developed as an alternative to previously reported routes from more sophisticated Ni(II) complexes:[4,5]

Nickelocene (500 mg, 2.65 mmol, 1 equiv) was weighed into a Teflon-stoppered ampoule and dissolved in THF (20 mL). The solution was cooled to –0 °C and PhLi (1.8 M solution in Bu_2O, 6 mL, 11 mmol, 4.2 equiv) was added dropwise. After 30 minutes of stirring at –40 °C, yellow microcrystals appeared, which were allowed to settle for some minutes. The reddish-brown solution was then separated from the yellow solid through filtration. After washing with cold pentane (5 mL) the pale-yellow solid was dried under vacuum. Yield = 500 mg (26%).

The complex was characterized by ^{1}H and ^{7}Li NMR spectroscopy. Yellow solutions in benzene became brown after 5 minutes at room temperature and biphenyl was detected by ^{1}H NMR spectroscopy. Identification of the complex as the reported species was further confirmed through X-ray diffraction studies of lustrous yellow crystals obtained from a THF solution at low temperature (−30 °C).[4,5]

^{1}H NMR (400 MHz, THF/C_6D_6, 25 °C): δ 8.30 (d, 8H, $^{3}J_{H\text{-}H}$ = 7 Hz, PhNi-*o*-C*H*), 7.05 (t, 8H, $^{3}J_{H\text{-}H}$ = 7 Hz, PhNi-*m*-C*H*), 6.80 (t, 4H, $^{3}J_{HH}$ = 7 Hz, PhNi-*p*-C*H*), 3.26 (br, OC*H*$_2$CH$_2$), 1.26 (OCH$_2$C*H*$_2$).

$^{7}Li\{^{1}H\}$ NMR (161 MHz, THF/C_6D_6, 25 °C): δ –1.20 (s).[1]

$Li_6(Et_2O)_4Ph_6Ni_2(C_6H_4)$ (5)

$Ni(COD)_2$ (86 mg, 0.313 mmol, 1 equiv) and $[PhLi]_\infty$ (131.9 mg, 0.782 mmol, 5 equiv) were weighed into an ampoule inside a N_2-filled glovebox. This was transferred to the Schlenk line and the atmosphere changed to Ar before the addition of degassed Et_2O (5 mL). The resulting red solution was heated at 33 °C for 22 h then volatiles removed to give a red residue. This was triturated with pentane (3 × 4 mL) until the residue was powdery and reddish brown. This residue contains excess PhLi and, often, a quantity of intermediate $[Li_2(THF)_4Ph_2Ni]_2COD$ (**2**).

*Complex **5** is best obtained through slow crystallisation:*

The powdery residue was dissolved in 2 mL Et_2O, filtered to remove any undissolved solid, then pentane (1 mL) added to this solution. Evaporation of *ca*. half the volatiles was followed by the addition of pentane (1 mL). Further concentration removing up to 1/3 of the solvent resulted in a red solution and orange solid ($[Li_2(THF)_4Ph_2Ni]_2COD$). Filtration through glass fibre filter paper was followed by slow evaporation of the pentane/Et_2O mixture at room temperature until half the solvents had evaporated. This was accompanied by the appearance of large dark brown-red crystals. At this point, the vial was loosely capped and placed in the glovebox freezer at −35 °C for 1 week. The supernatant was removed and the dark red crystals washed with pentane (2 mL) then dried under vacuum. Yield = 37.8 mg (25%).

Removal of PhLi can also be achieved by slow evaporation (8 weeks) of a 1:1 hexane/ether solution at −30 °C (reaction at 1 mmol scale = 2 mL of each solvent). The fine off-white precipitate of PhLi remains suspended in hexane, whilst the large crystals of **5** stay at the bottom of the vial, enabling the two species to be physically separated by “crystal panning”. Yield for a 1 mmol scale = 52 mg (10%). Slightly improved yields (15–21%) were obtained when the reaction was performed on a 0.36 mmol scale (100 mg of $Ni(COD)_2$).

*N.B. The low yields of **5** are primarily attributed to challenges associated with removal of excess PhLi and trace **2**. NMR spectroscopic monitoring of the reaction mixture indicates that **5** is the major species.*

[1] The difference in the ^{7}Li NMR chemical shift between the already reported $[Li_2NiPh_4(THF)_4]$ might be due to the formation in our case of the solvent separated pair species $[Ni(C_6H_5)_4]^{2-}[Li(THF)_x]_2^{2+}$ where the Li is surrounded by more than two THF molecules.

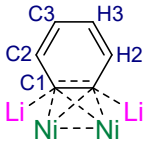

^{1}H NMR (400 MHz, THF-d_8, 25 °C): δ 8.11 (br s, $\Delta\nu_{1/2}$ = 18 Hz, 8 H, PhNi-*o*-C*H*), 7.81 (d, 4 H, $^{3}J_{H–H}$ = 6.2 Hz, PhLi-*o*-C*H*), 6.77 (t, 4 H, $^{3}J_{H-H}$ = 6.8 Hz, PhLi-*m*-C*H*), 6.67–6.60 (m, 10 H, *H*3-C_6H_4, PhNi-*m*-C*H* and PhLi-*p*-C*H*), 6.48 (t, 4 H, $^{3}J_{H-H}$ = 7.3 Hz, PhNi-*p*-C*H*), 5.77 (dd, 2H, J_{H-H} = 5.2, 2.3 Hz, *H*2–C_6H_4), 3.39 (q, $^{3}J_{H-H}$ = 7.0 Hz, Et_2O), 1.12 (t, $^{3}J_{H-H}$ = 7.0 Hz, Et_2O).

^{13}C{^{1}H} NMR (100 MHz, THF-d_8, 25 °C): δ 191.8 (PhLi-*ipso*-*C*), 185.3 (PhNi-*ipso*-*C*), 143.7 (PhNi-*o*-*C*), 143.6 (PhLi-*o*-*C*), 125.6 (PhNi-*m*-*C*), 124.9 (*C*3–C_6H_4),124.5 (PhLi-*m*-*C*), 122.0 (PhLi-*p*-*C*), 120.2 (PhNi-*p*-*C*), 115.5 (*C*2–C_6H_4), 71.5 (*C*1–C_6H_4), 66.1 (Et_2O), 15.5 (Et_2O).

^{7}Li{^{1}H} NMR (161 MHz, THF-d_8, 25 °C): δ −1–2 (br m);
^{7}Li{^{1}H} NMR (161 MHz, THF-d_8, −80 °C): δ 1.28 (s), 0.85 (s), −0.68 (s) (1:1:1 ratio).

Elemental analysis (%): Calc. for $C_{58}H_{74}Li_6Ni_2O_4$: C, 70.07; H, 7.50; Expt.: C, 70.35; H, 7.24.

$Li_5(THF)_5Ph_5Ni_2(C_6H_4)$ (6)

A Schlenk flask charged with a glass-coated stir bar, $Ni(COD)_2$ (100 mg, 0.36 mmol, 1 equiv) and PhLi(THF) (170 mg, 1.20 mmol, 3.3 equiv) was cooled to −30 °C and toluene (5 mL) was slowly added. The reaction mixture was then warmed to room temperature and stirred for 16 hours to give a dark red solution. The volatiles were removed *in vacuo* and the residues were washed with hexane (1 mL), then extracted into hexane (1 mL) and Et_2O (1 mL) and filtered through a Celite/glass wool plug. The filtrate was stored in the glovebox freezer (−30 °C) for 24 hours affording dark red blocky crystals of **6**. The supernatant was decanted and the solids were washed with cold hexane (2 × 0.5 mL) and dried under argon. Yield = 89 mg (50%).

^{1}H NMR spectroscopy indicates a mixed THF/Et_2O solvate of the approximate bulk constitution $Li_5(THF)_{2.9}(Et_2O)_{1.3}Ph_5Ni_2(C_6H_4)$.

^{1}H NMR (300 MHz, THF-d_8, 25 °C): δ 8.13 (br d, 8H, $^{3}J_{H-H}$ = 5.9 Hz, PhNi-*o*-C*H*), 7.86 (d, 2H, $^{3}J_{H-H}$ = 6.0 Hz, PhLi-*o*-C*H*), 6.81 (t, 2H, $^{3}J_{H-H}$ = 6.9 Hz, PhLi-*m*-C*H*), 6.74–6.64 (m, 11H, *H*3-C_6H_4, PhNi-*m*-C*H*, PhLi-*p*-C*H*), 6.54–6.45 (m, 4H, PhNi-*p*-C*H*), 5.78 (dd, 2H, $^{3}J_{H-H}$ = 5.5, 2.5 Hz, *H*2-C_6H_4), 3.62 (m, THF), 3.39 (q, $^{3}J_{H-H}$ = 7.0 Hz, Et_2O), 1.78 (m, THF), 1.12 (t, $^{3}J_{H-H}$ = 7.0 Hz, Et_2O).

^{13}C{^{1}H} NMR (75.5 MHz, THF-d_8, 25 °C): δ 190.8 (PhLi-*ipso*-*C*), 185.6 (PhNi-*ipso*-*C*), 144.1 (PhLi-*o*-*C*H), 144.0 (PhNi-*o*-*C*H), 126.0 (PhNi-*m*-*C*H), 125.2 (*C*3-C_6H_4), 125.0 (PhLi-*m*-*C*H), 122.7 (PhLi-*p*-*C*H), 120.5 (PhNi-*p*-*C*H), 115.8 (*C*2-C_6H_4), 71.9 (*C*1-C_6H_4), 68.4 (THF), 66.5 (Et_2O), 26.5 (THF), 15.9 (Et_2O).

^{7}Li{^{1}H} NMR (155.5 MHz, THF-d_8, −40 °C): δ 1.39, 0.99, −0.59 (1:2:2 ratio).

Elemental Analysis: Calc. for $C_{56}H_{69}Li_5Ni_2O_5$: C, 69.04; H, 7.14. Found: C, 68.70; H, 7.43.

$[Li_2(THF)_4NiPh_4]$ + PhLi

$[Li_2(THF)_4NiPh_4]$ (100 mg, 0.14 mmol, 1 equiv) and $[(PhLi{\cdot}OEt_2)_4]$ (44 mg, 0.07 mmol, 0.5 equiv) were placed in an ampoule under an Ar atmosphere, cooled to 0 °C then suspended in Et_2O (15 mL). The mixture was allowed to stir to room temperature for 48 hours, during which time it became a dark red solution. After removing the solvent under vacuum, the red residue dissolved both in benzene-d_6 (Figure S1) and THF-d_8 (Figure S2) observing the formation of complex **5** as the major product of the reaction, alongside biphenyl.

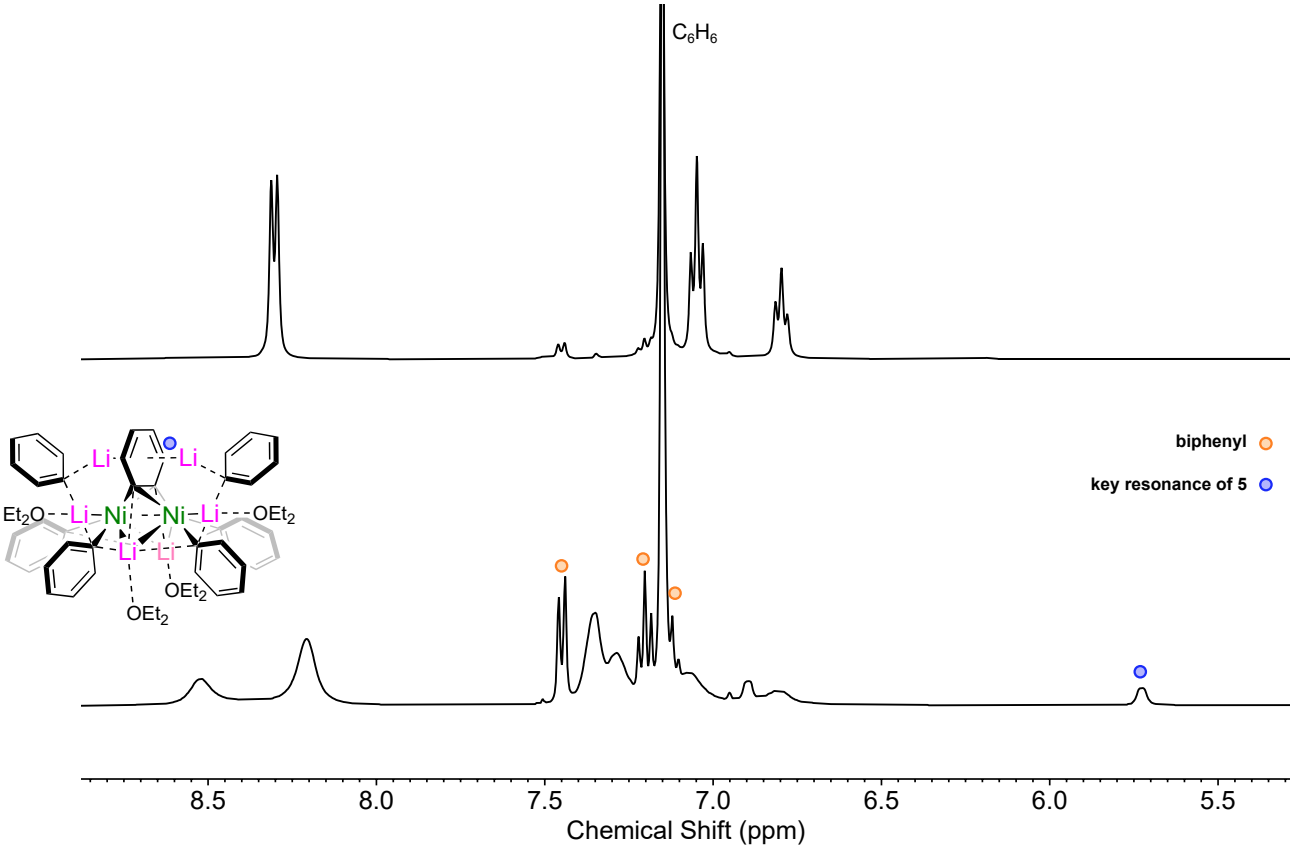

Figure S1: $[Li_2(THF)_4NiPh_4]$ in THF-d_8 (top); **$[Li_2(THF)_4NiPh_4]$ + PhLi (2 equiv)** in THF-d_8 (bottom).

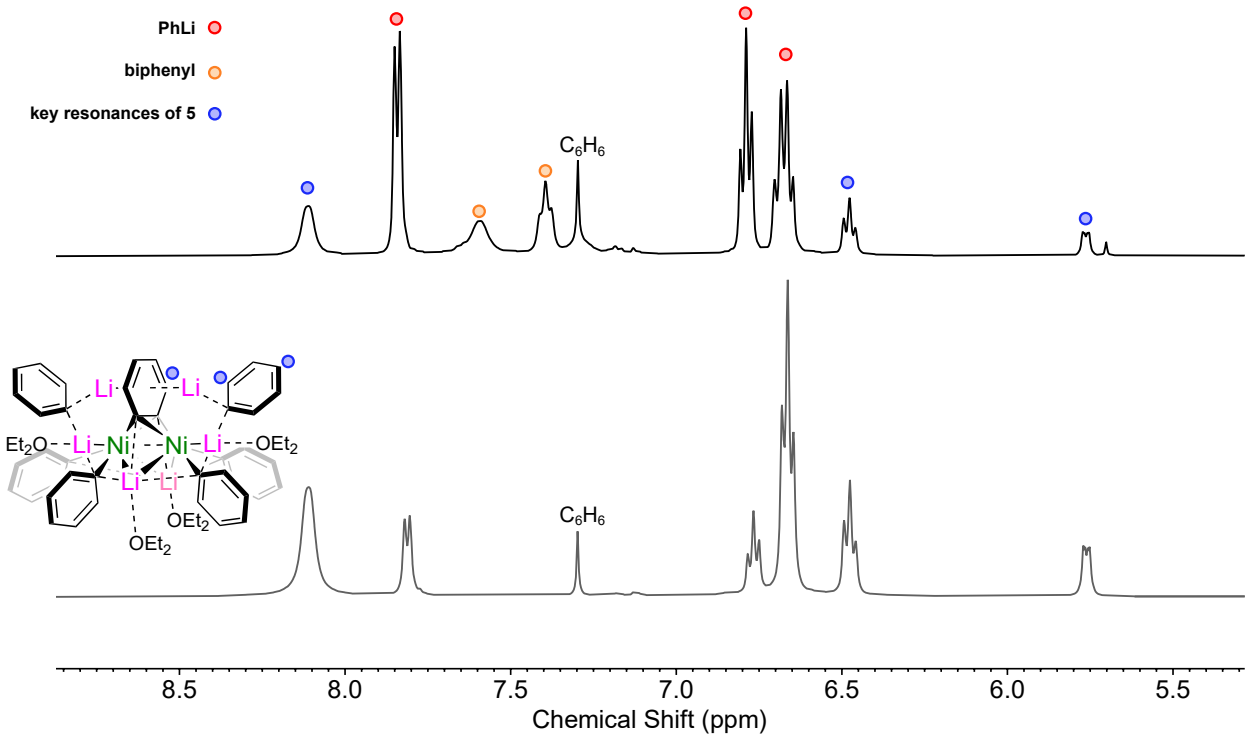

Figure S2: $[Li_2(THF)_4NiPh_4]$ + PhLi in THF-d_8, 48 h (top); complex **5** in THF-d_8 (bottom).

PhNa

Caution: PhNa is pyrophoric!

PhLi (500 mg, 5.9 mmol, 1 equiv) and NaO^{t}Bu (572 mg, 5.9 mmol, 1 equiv) were combined in hexane (20 mL) at 0 °C then warmed to room temperature and stirred for 24 hours to give a pale pink suspension. The solids were collected on a glass sintered filter frit, washed with pentane (2 × 5 mL), and dried *in vacuo*. Yield = 590 mg (99%).

^{1}H NMR (300 MHz, THF-H_8): δ 7.82 (m, 2H, *o-Ph*), 6.80 (m, 2H, *m-Ph*), 6.69 (m, 1H, *p-Ph*). PhNa rapidly decomposes in THF, and signals corresponding to C_6H_6 and ethene, amongst other unidentified signals are observed.

$[Na_2(solv)_3Ph_2Ni(olefin)]_2$ (7)

A Schlenk flask charged with a glass-coated stir bar, $Ni(COD)_2$ (75 mg, 0.27 mmol, 1 equiv) and PhNa (55 mg, 0.55 mmol, 2 equivalents) was cooled to −30 °C and Et_2O (5 mL) was slowly added. The reaction mixture was then warmed to room temperature and stirred for 30 minutes to give an orange solution. The volatiles were removed *in vacuo* and the residues were washed with hexane (1 mL), then extracted into hexane (1 mL) and Et_2O (1 mL) and filtered through a Celite/glass wool plug. The filtrate was stored in the glovebox freezer (−30 °C) for 48 hours affording a pale orange microcrystalline solid. The

supernatant was decanted and the solids were washed with cold hexane (2 × 0.5 mL) and dried under argon. Yield = 52 mg (40%). Single crystals suitable for X-ray diffraction were grown from THF/hexane at −30 °C.

Although COD is coordinated to Ni in the solid-state structure, isolated material was found to instead contained coordinated C_2H_4 by NMR spectroscopy, and matches the previously reported literature values.[6,7] The C_2H_4 ligand is proposed to originate from decomposition and cleavage of Et_2O or THF.

^{1}H NMR (300 MHz, THF-d_8, 25 °C): δ 8.08 (d, 4H, $^3J_{H\text{-}H}$ = 6.3 Hz, PhNi-*o*-C*H*), 6.69 (t, 4H, $^3J_{H\text{-}H}$ = 7.2 Hz, PhNi-*m*-C*H*), 6.48 (t, 2H, $^3J_{H\text{-}H}$ = 7.2 Hz, PhNi-*p*-C*H*), 3.39 (q, $^3J_{H\text{-}H}$ = 7.0 Hz, Et_2O), 1.12 (t, $^3J_{H\text{-}H}$ = 7.0 Hz, Et_2O), 0.46 (s, 4H, C_2H_4).

^{13}C{^{1}H} NMR (75.5 MHz, THF-d_8, 25 °C): δ 192.9 (PhNi-*ipso*-*C*), 142.9 (PhNi-*o*-*C*H), 125.9 (PhNi-*m*-*C*H), 119.2 (PhNi-*p*-*C*H), 66.5 (Et_2O), 21.1 (C_2H_4), 15.9 (Et_2O).

Due to the extreme sensitivity of this compound, it was not possible to get satisfactory elemental analysis.

$[Na_2(Et_2O)_3Ph_2(NaC_8H_{11})NiCOD]_2$ (8)

A Schlenk flask charged with a glass-coated stir bar, $Ni(COD)_2$ (100 mg, 0.36 mmol, 1 equiv) and PhNa (120 mg, 1.20 mmol, 3.3 equivalents) was cooled to −30 °C and Et_2O (10 mL) was slowly added. The reaction mixture was then warmed to room temperature and stirred for 90 minutes to give a deep red solution. The volatiles were removed *in vacuo* and the residues were washed with hexane (1 mL), then extracted into hexane (1 mL) and Et_2O (1 mL) and filtered through a Celite/glass wool plug. The filtrate was stored in the glovebox freezer (−30 °C) for 1 week affording orange crystals suitable for single-crystal X-ray diffraction studies, identified as $[Na_2(Et_2O)_3Ph_2(NaC_8H_{11})NiCOD]_2$. Attempts to isolate **8** in pure form were unsuccessful however, and analysis by NMR spectroscopy showed that **7** was the major species.

NMR Studies

DOSY NMR Studies on 5

Estimated molecular weights (MW) were calculated from the diffusion coefficients established from the ^{1}H DOSY NMR spectrum using Stalke's external calibration curve (ECC) method against the normalised diffusion coefficient for the internal reference (Me_4Si).[8–10] A 0.015 M solution was prepared by dissolving 7.7 mg (0.0075 mmol) of **5** in 0.5 mL of THF-d_8 along with tetramethylsilane (1 µL, 0.0075 mmol). Multiple non-overlapping ^{1}H NMR signals were used to calculate the average diffusion coefficient for each species in solution, and the molecular weight was estimated using the dissipated spheres and ellipsoids (DSE) option, which has been reported to be the most appropriate option for organometallic compounds.[10]

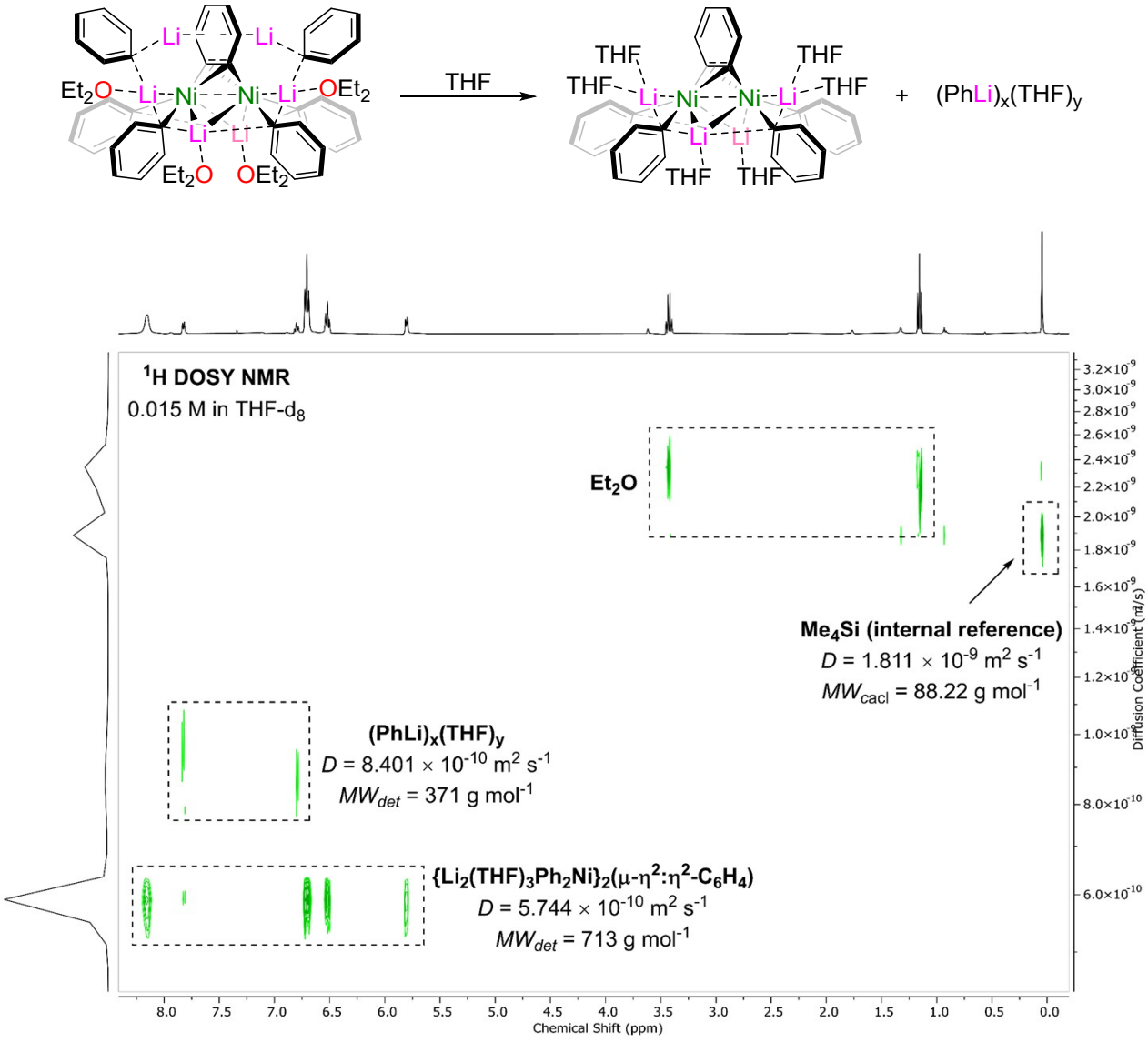

Figure S3: ^{1}H DOSY NMR spectrum of **5** in THF-d_8 (0.015 mM).

Determined molecular weight for the $(PhLi)_x(THF)_y$ component from diffusion coefficients = 371 g mol^{-1}; expected molecular weight for $[PhLi(THF)_2]_2$ = 456.52 g mol^{-1}; expected molecular weight for $[PhLi(THF)_3]$ = 300.37 g mol^{-1}. PhLi exists as a mixture of disolvated dimers and trisolvated monomers

in bulk THF, and this is consistent with the estimated molecular weight from the diffusion coefficient which is midway between these values. Determined molecular weight for the $Li_4(THF)_xPh_4Ni_2(C_6H_4)$ component from diffusion coefficients = 713 g mol^{-1}; expected molecular weight for $Li_4(THF)_6Ph_4Ni_2(C_6H_4)$ = 818.10 g mol^{-1} (15% difference). Although the ECC method is not yet optimised for aggregates with MWs > 600 g mol^{-1}, the DOSY NMR spectra nevertheless provides strong support for the dissociation of PhLi from the cluster in bulk THF.

NOE and EXSY NMR Studies on 5

A series of $^1H\{^1H\}$ NOE NMR experiments were first performed to assess possible exchange processes in compound **5** (**Figure S4**). Selective irradiation of the *o*-C*H* protons (δ 7.81) of the $(PhLi)_x(THF)_y$ component identified that these were in dynamic exchange with the *o*-C*H* protons (δ 8.81) of the $Li_4(THF)_xPh_4Ni_2(C_6H_4)$ component, with an NOE correlation (opposite phase) to the *m*-C*H* protons (δ 6.76) of the $(PhLi)_x(THF)_y$ component (spectrum b). Selective irradiation of the *H*2-C_6H_4 protons (δ 5.76) identified no exchange with 'PhLi' or 'PhNi', and only an NOE correlation to the *H*3-C_6H_4 protons was observed (spectrum c).

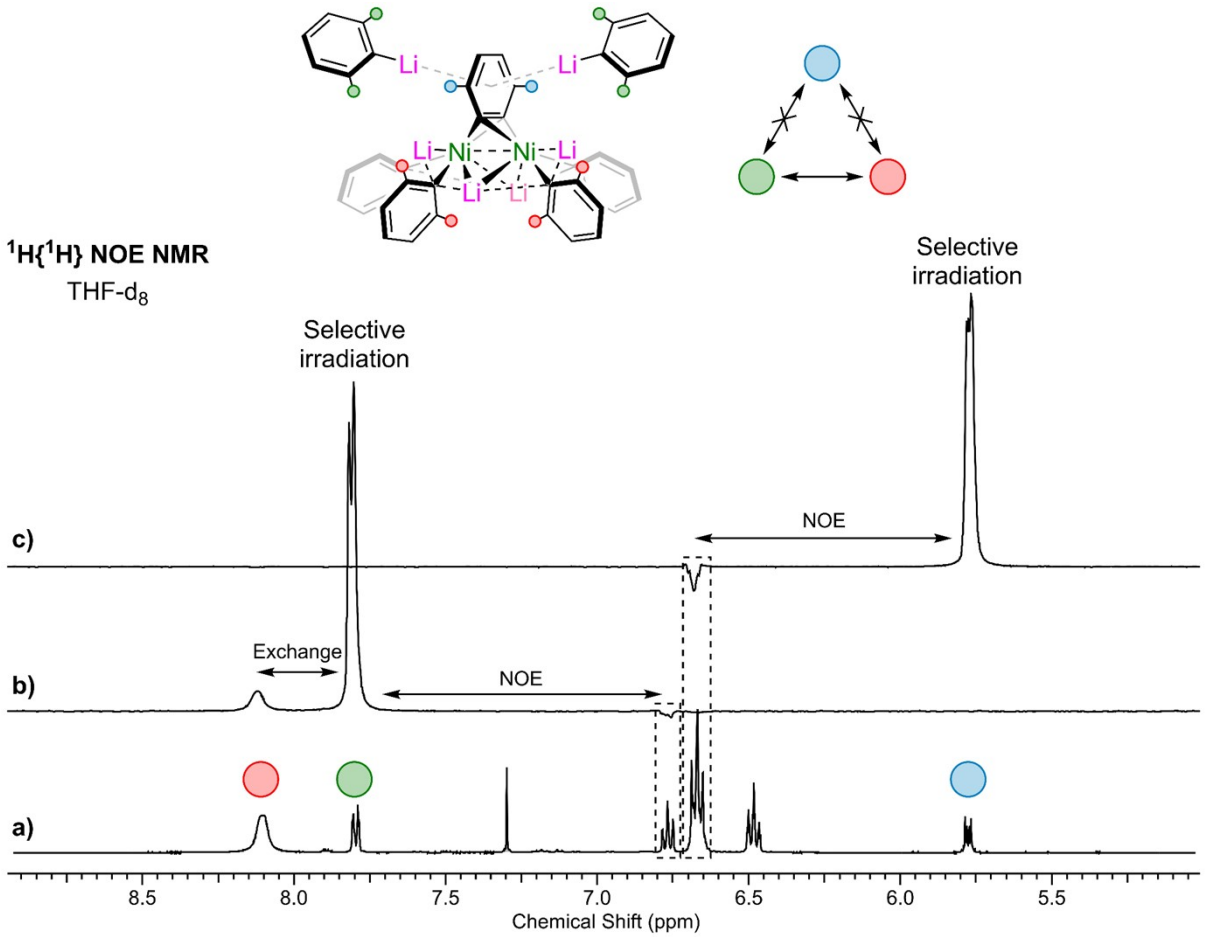

Figure S4: ^1H NMR spectrum of **5** in THF-d_8; b) $^1H\{^1H\}$ NOE NMR spectrum of 5 with selective irradiation at 7.81 ppm; c) $^1H\{^1H\}$ NOE NMR spectrum of 5 with selective irradiation at 5.76 ppm.

An ^{1}H-^{1}H EXSY NMR experiment was performed to further confirm the exchange process between dissociated PhLi and the lithium nickelate (**Figure S5**). The off-diagonal cross-peaks correspond to exchanging spins.

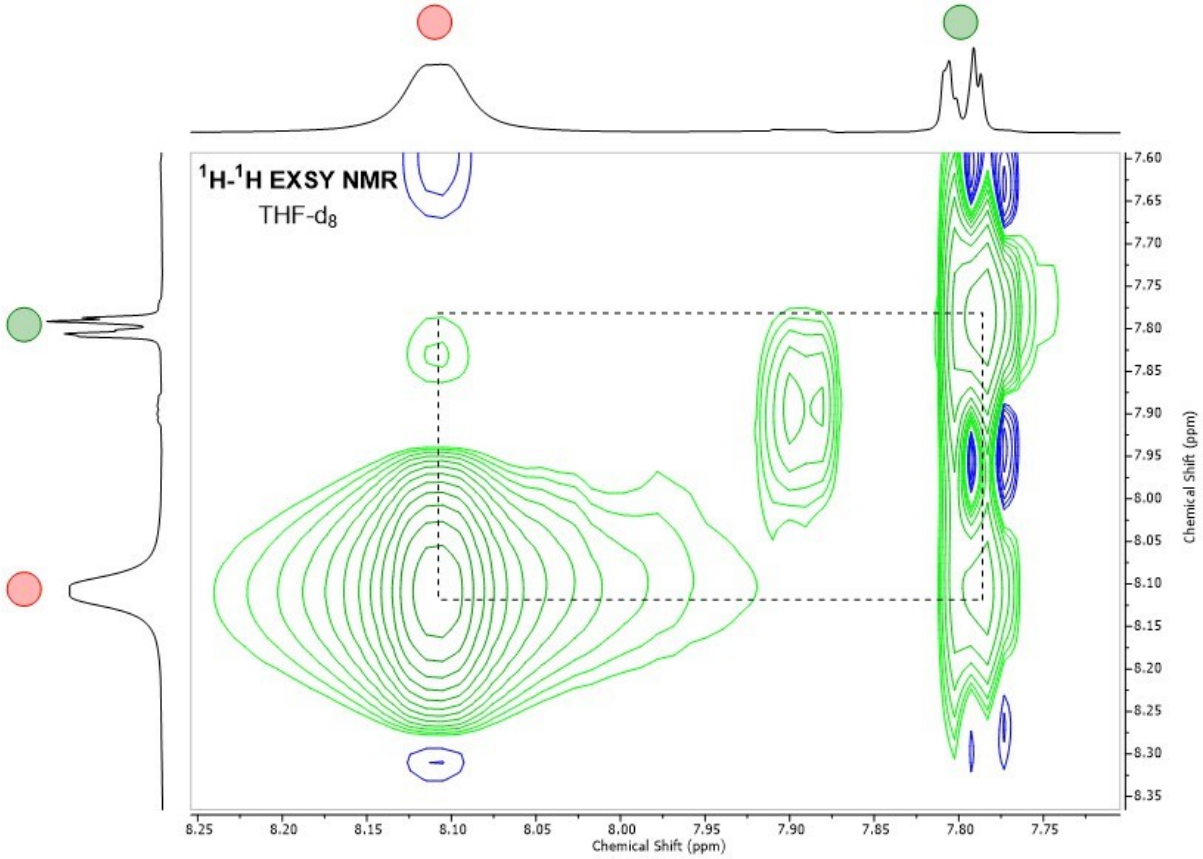

Figure S5: ^{1}H–^{1}H EXSY NMR spectrum of **5** in THF-d$_8$.

Variable Temperature NMR Studies on 5 and 6

Crystalline **5** (20 mg) and **6** were separately dissolved in THF-d$_8$ (0.5 mL) and analysed by ^{1}H and ^{7}Li{^{1}H} NMR spectroscopy at +20 °C, 0 °C, −20 °C, −40 °C, −60 °C and −80 °C (**Figure S6–Figure S9**). On cooling to −80 °C, the broad signal for the PhNi-*o*-C<u>*H*</u> protons has decoalesced into two well resolved doublets at δ 8.49 ($^{3}J_{H\text{-}H}$ = 6.9 Hz) and δ 7.68 ($^{3}J_{H\text{-}H}$ = 6.7 Hz) due to lack of rotation around the Ni-C$_{ispo}$ bond. The PhNi-*m*-C<u>*H*</u> protons also resolve into two separate broad triplets at δ 6.65 ($^{3}J_{H\text{-}H}$ ≈ 6.5 Hz) and δ 6.49 ($^{3}J_{H\text{-}H}$ ≈ 6.9 Hz), and the <u>*H*</u>3-C$_6$H$_4$ signal becomes visible at δ 6.54 (dd, $^{3}J_{H\text{-}H}$ = 5.5, 2.5 Hz).

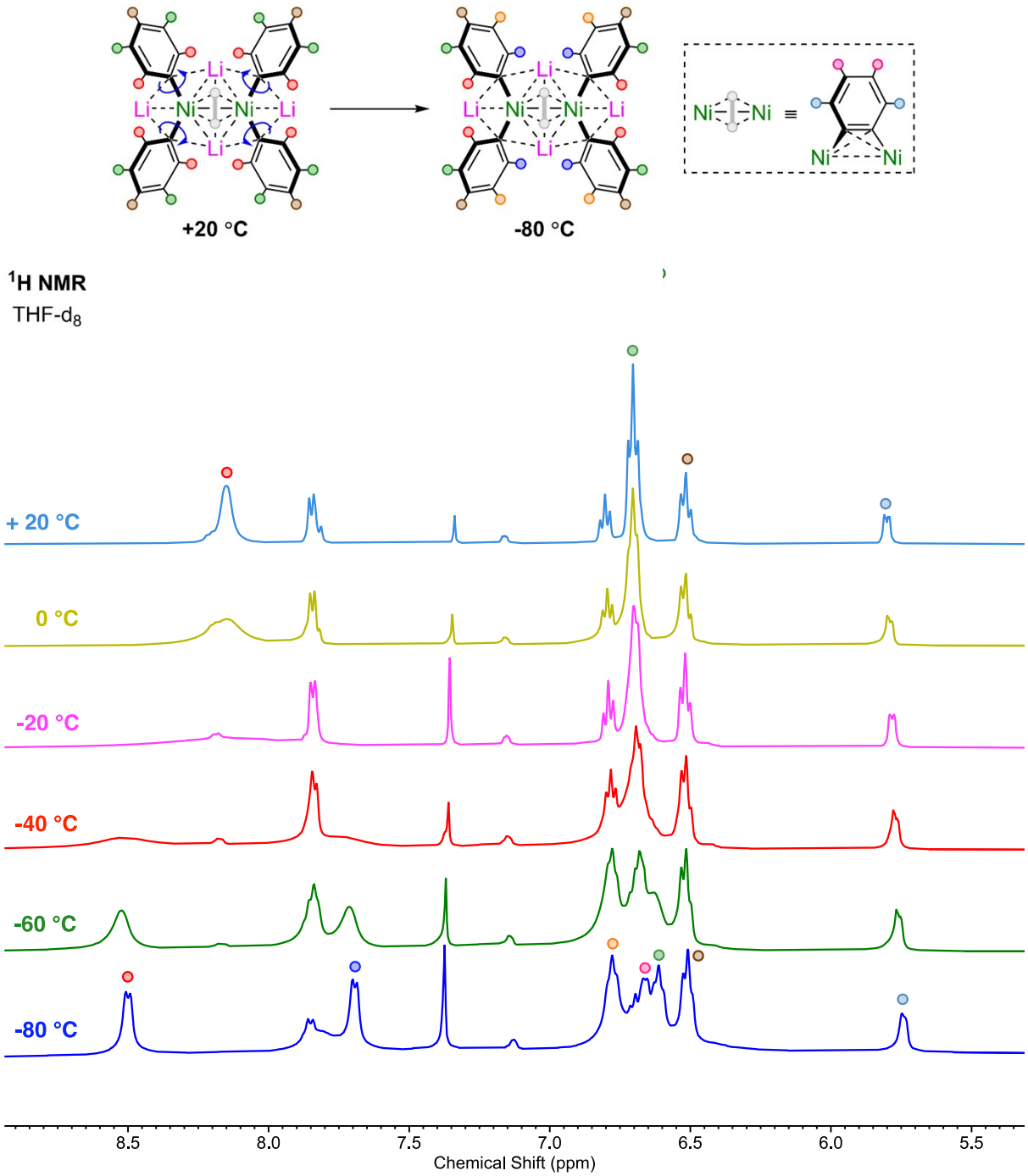

Figure S6: Stacked ^{1}H NMR spectra of **5** in THF/THF-d$_8$ (3:1) at variable temperatures.

The room temperature ^{1}H NMR spectrum of **6** closely resembles compound **5**, which is consistent with dissociation of PhLi in solution to give a C_{2v} symmetric $Li_4(THF)_xPh_4Ni_2(C_6H_4)$ species.

Figure S7: Stacked ^{1}H NMR spectra of **6** in THF-d_8 at variable temperatures.

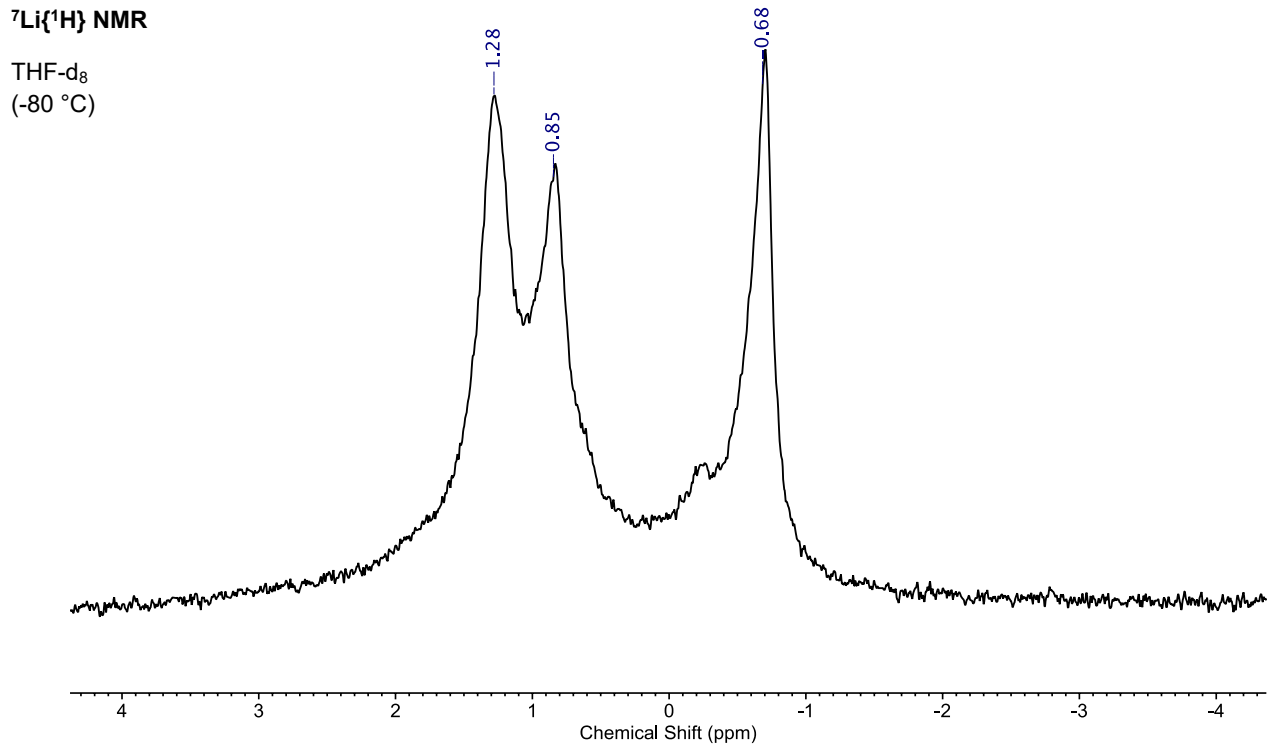

Figure S8. $^{7}Li\{^{1}H\}$ NMR spectrum of **2** in THF-d_8 at −80 °C.

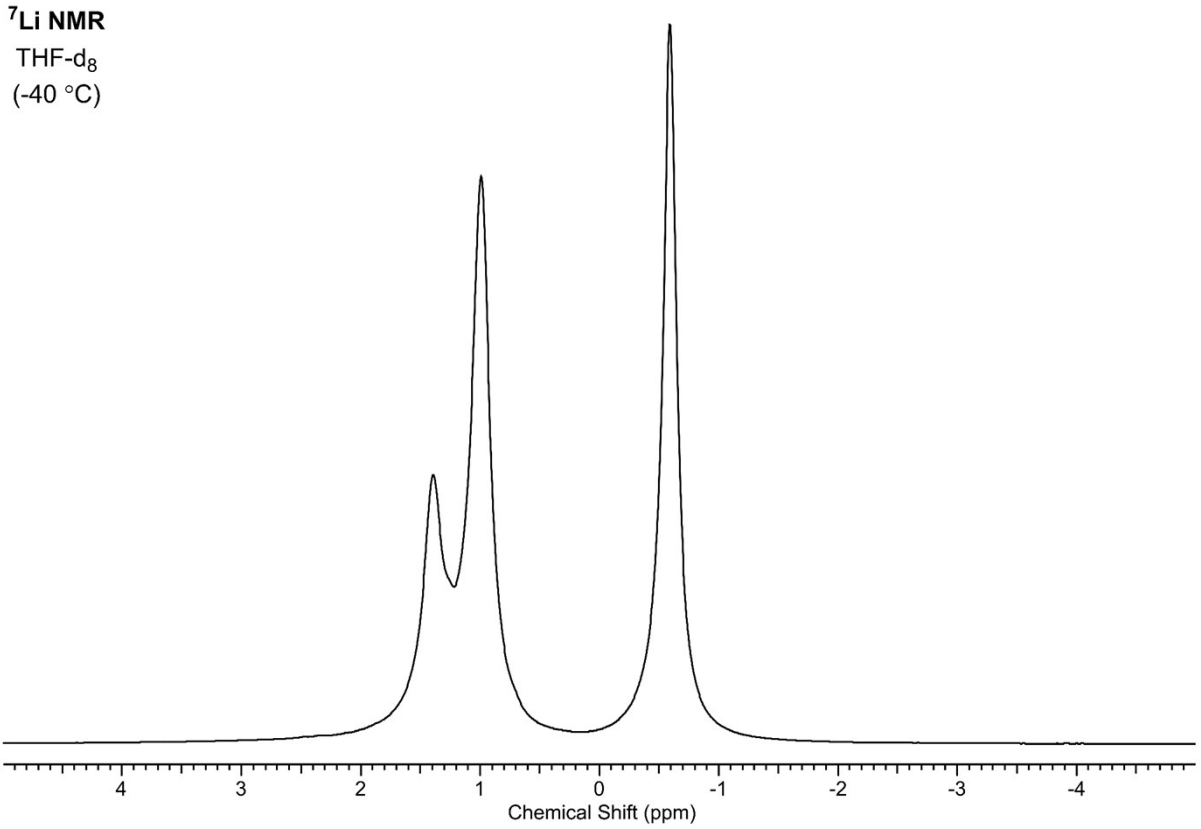

Figure S9: ^{7}Li NMR spectrum of **6** in THF-d_8 at −40 °C.

Crystalline **5** (15 mg) was also dissolved in toluene-d_8 (0.5 mL) and Et_2O (50 µL), and analysed by ^1H and ^7Li NMR spectroscopy at +20 °C, 0 °C, −20 °C, −40 °C, −60 °C and −80 °C (**Figure S10** and **Figure S11**). The solution-state behaviour of **5** in toluene/Et_2O suggests a fluxional process which likely originates from partial 'PhLi' dissociation (*vide supra*). It is evident from the ^1H and ^7Li NMR spectra at low temperatures that the *pseudo*-C_{2v} symmetric structure that is observed in the solid state is not retained in solution. The 5 unique signals observed in the ^7Li NMR spectrum are consistent with a structure similar to **6** in the solid-state.

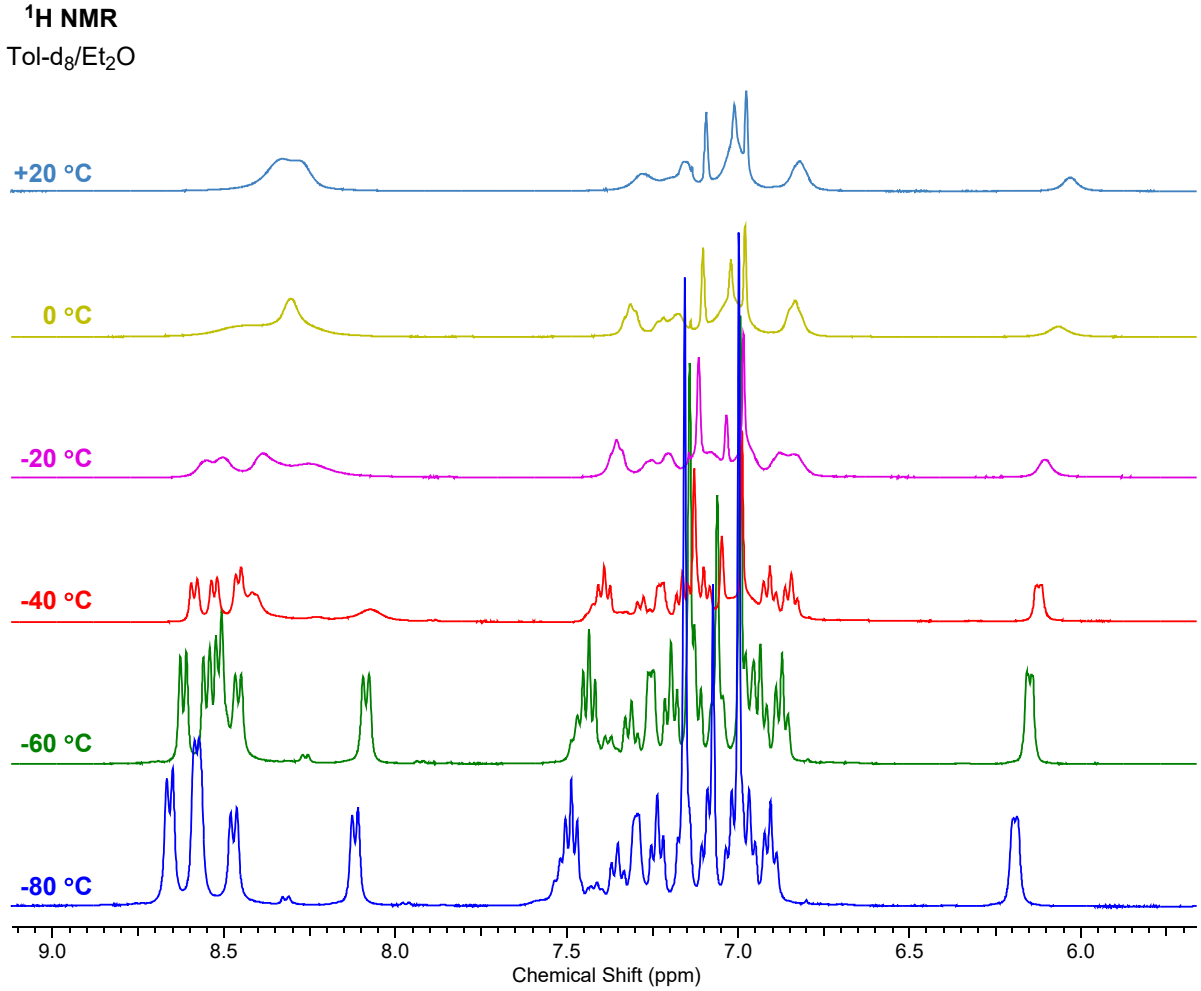

Figure S10: Stacked ^1H NMR spectra of **5** in Tol-d_8/Et_2O at variable temperatures.

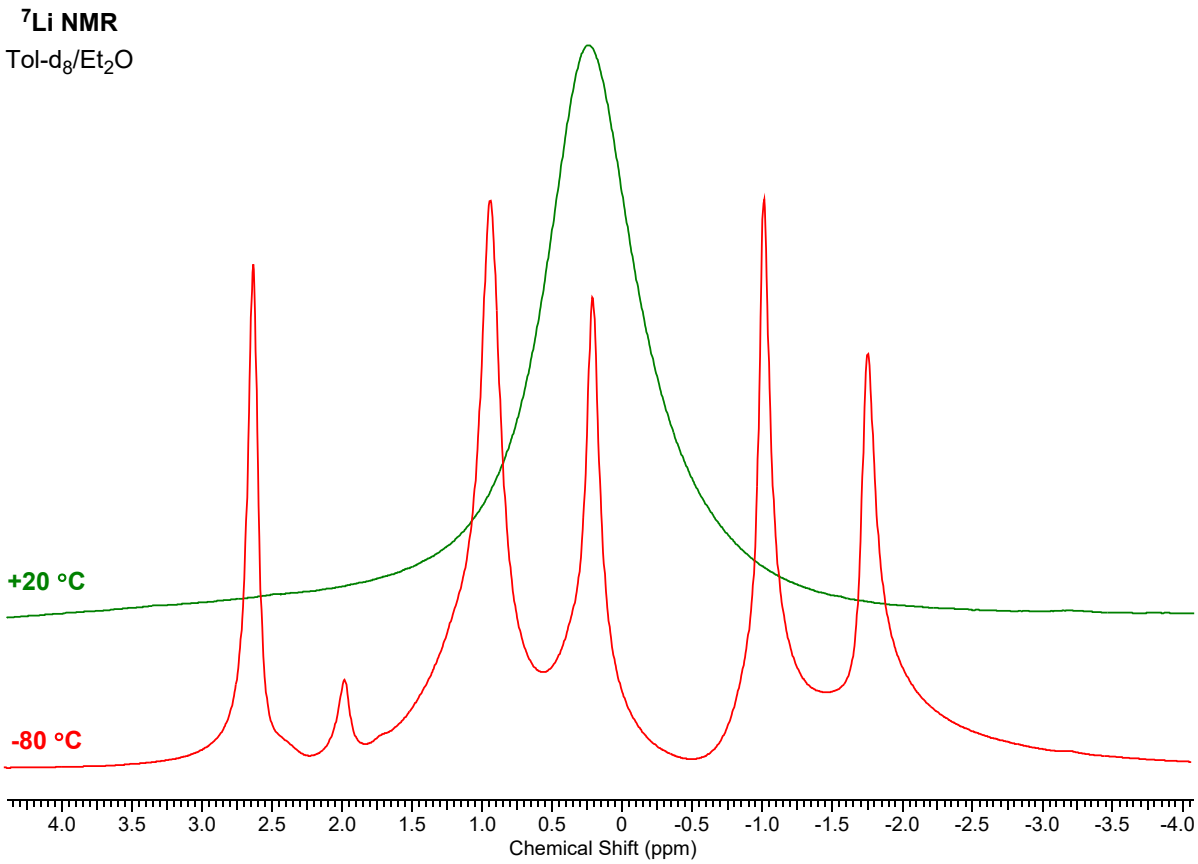

Figure S11: Stacked ^{7}Li NMR spectra of **5** in Tol-d_8/Et_2O at +20 °C and −80 °C.

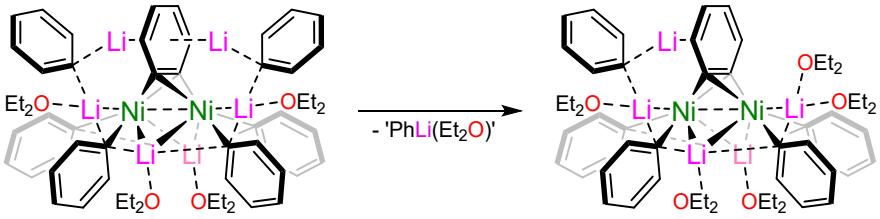

Figure S12: Proposed 'PhLi' dissociation from **5** accounting for the five signals observed in the ^{7}Li NMR spectrum at low temperatures.

LiH Trapping Reactions

Attempted Trapping with BH_3

$Ni(COD)_2$ (20 mg, 0.073 mmol) and PhLi (21.4 mg, 0.254 mmol, 3.5 equiv) were combined in a mixture of toluene-d_8 (0.5 mL) and Et_2O (50 μL). This was then heated at 33 °C for 22 hours to give a deep red solution. ^1H NMR analysis indicated the formation of **5**, as evidenced by the characteristic benzyne multiplet at 6.00 ppm (**Figure S13**). BH_3.THF (1 M solution, 36 μL, 0.5 equiv) was then added. ^{11}B NMR spectroscopy shows the formation of BH_4^- - this gives a pentet at -41.95 ppm that collapses to a singlet in the $^{11}B\{^1H\}$ NMR spectrum (**Figure S14**). Many other boron-containing species are observed however due to the competing reaction between BH_3 and COD or PhLi.

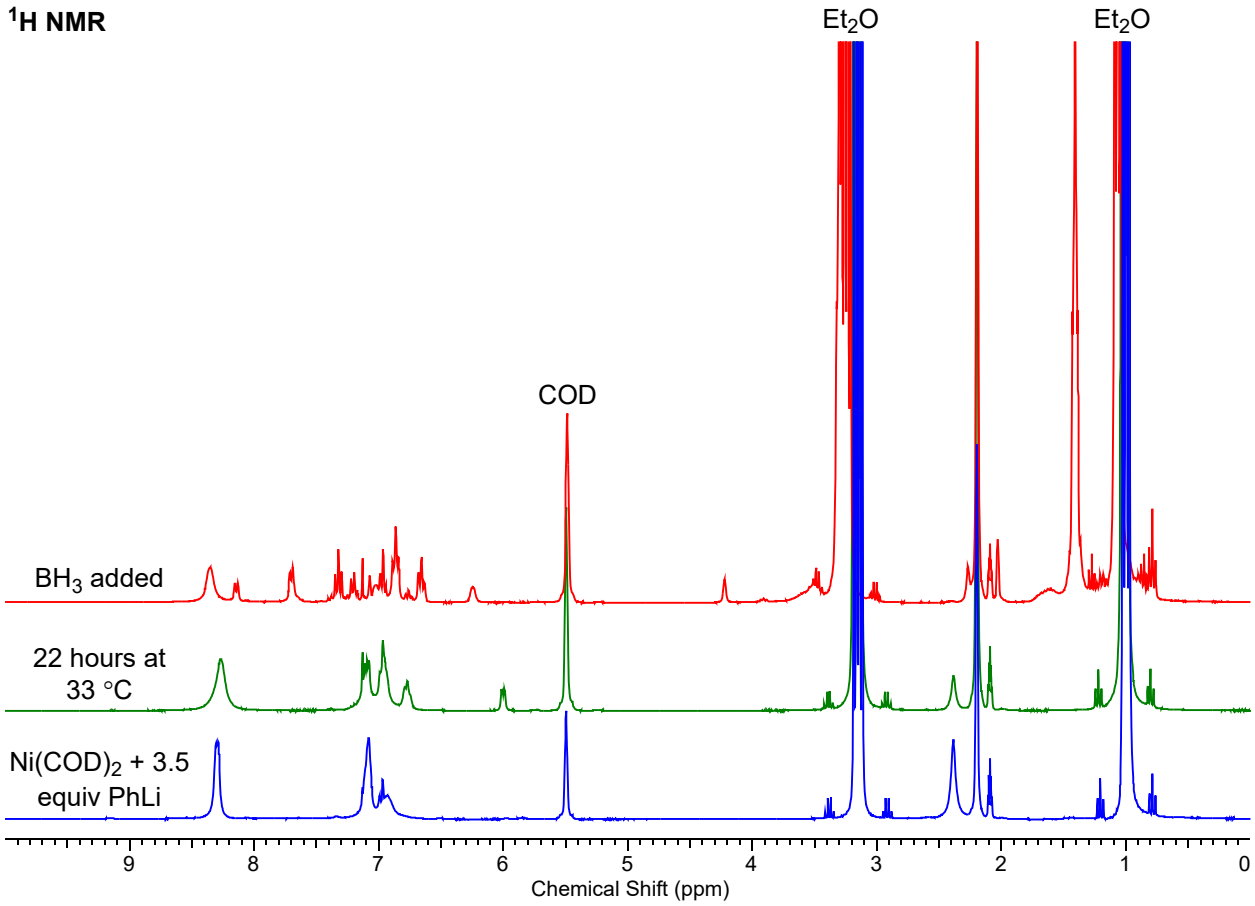

Figure S13: Stacked ^1H NMR spectra showing the *in situ* formation of **5** and its reaction with BH_3.

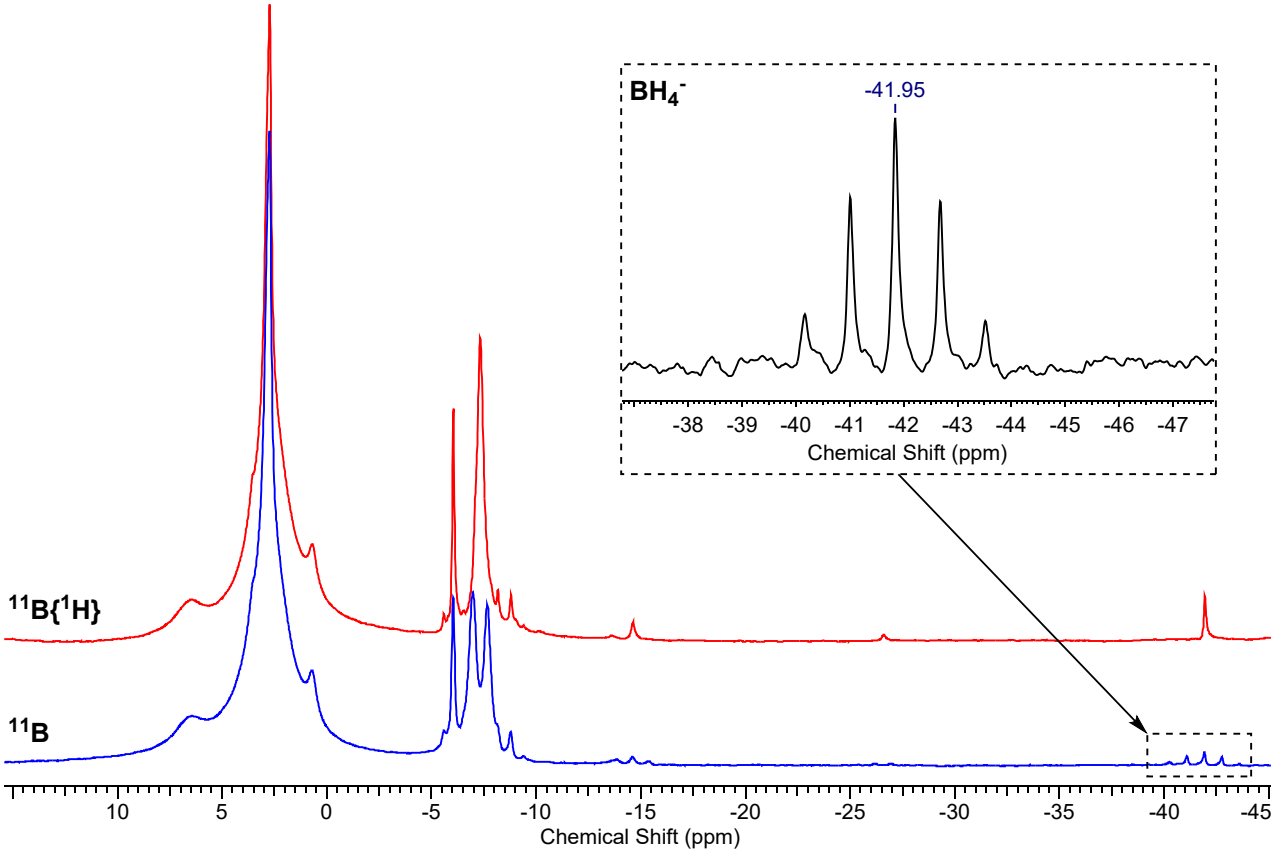

Figure S14: ^{11}B and $^{11}B\{^1H\}$ NMR spectra showing the reaction of **5** with BH_3.

Attempted Trapping with Benzophenone

$Ni(COD)_2$ (20 mg, 0.073 mmol) and PhLi (24.5 mg, 0.291 mmol, 4 equiv) were dissolved in Et_2O (0.5 mL) and heated at 33 °C for 22 hours to give a deep red solution. The solvent was removed *in vacuo* and the residues redissolved in THF-d_8 (0.5 mL). ^1H NMR analysis indicated the formation of **5** as evidenced by a characteristic benzyne signal at 5.77 ppm. Excess benzophenone (53 mg, 0.291 mmol) was added causing an immediate colour change from deep red to deep blue/teal, characteristic for the benzophenone ketyl radical anion. 1H NMR analysis only showed broad, unresolved signals with no unambiguous evidence for the formation of the 1,2-hydrolithiation product, $Ph_2C(H)OLi$.

^{1}H NMR

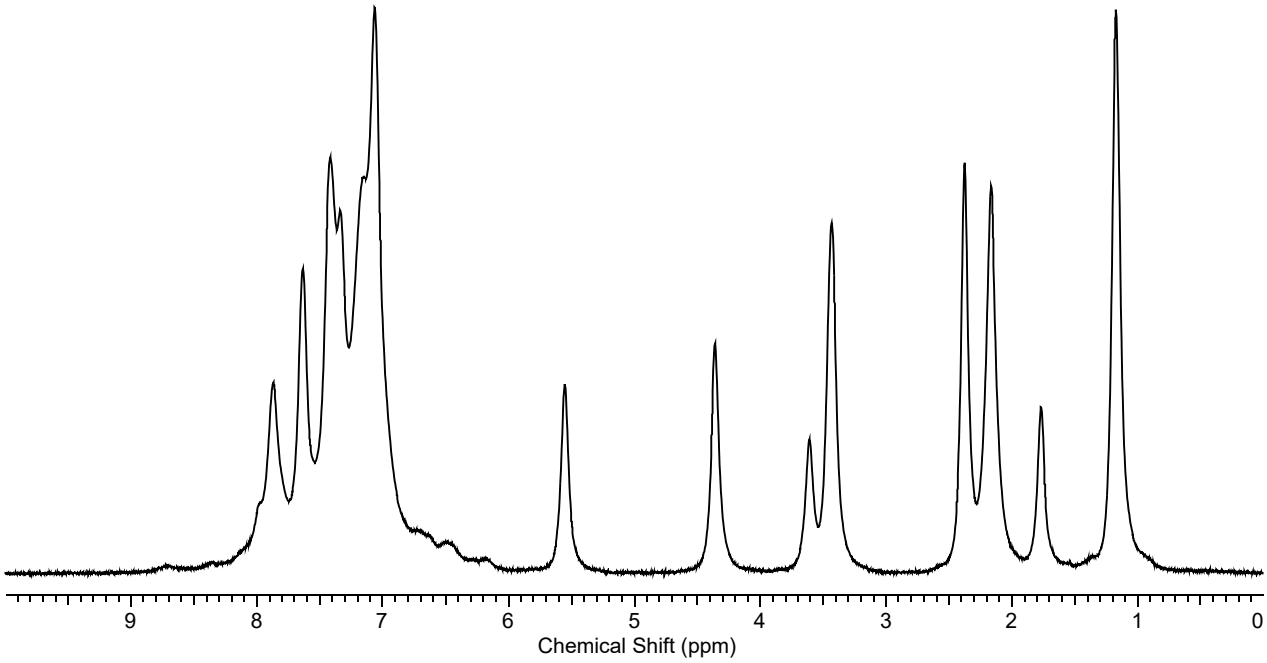

Figure SX: ^{1}H NMR spectrum on addition of benzophenone to *in situ* synthesised **5**.

Stoichiometric reactivity of 5 and 6

Complex **5** or **6** (4–8 mg) was dissolved in a 3:1 mixture of THF/THF-d_8 (0.5 mL). The substrate was added either in excess (I_2, MeI, anthracene), or 1 equiv (anthracene). GC–MS samples were prepared by diluting the NMR samples with 3 parts EtOAc then passing the mixture through 1 cm of silica (under air).

I_2

As reported by Taube, ^{1}H NMR and GC-MS showed formation of biphenyl upon reaction of I_2 with **6**. We also detected the formation of *o*-terphenyl, presumably from elimination of the bridging moiety and phenyl ligands. We estimated the conversion of the bridging moiety to *o*-terphenyl to be 50% (CH_2Cl_2 capillary as internal standard).

Biphenyl/o-terphenyl ratio of 3:1. Remaining phenyl groups found as C_6H_6, which overlaps with signals of biphenyl and *o*-terphenyl.

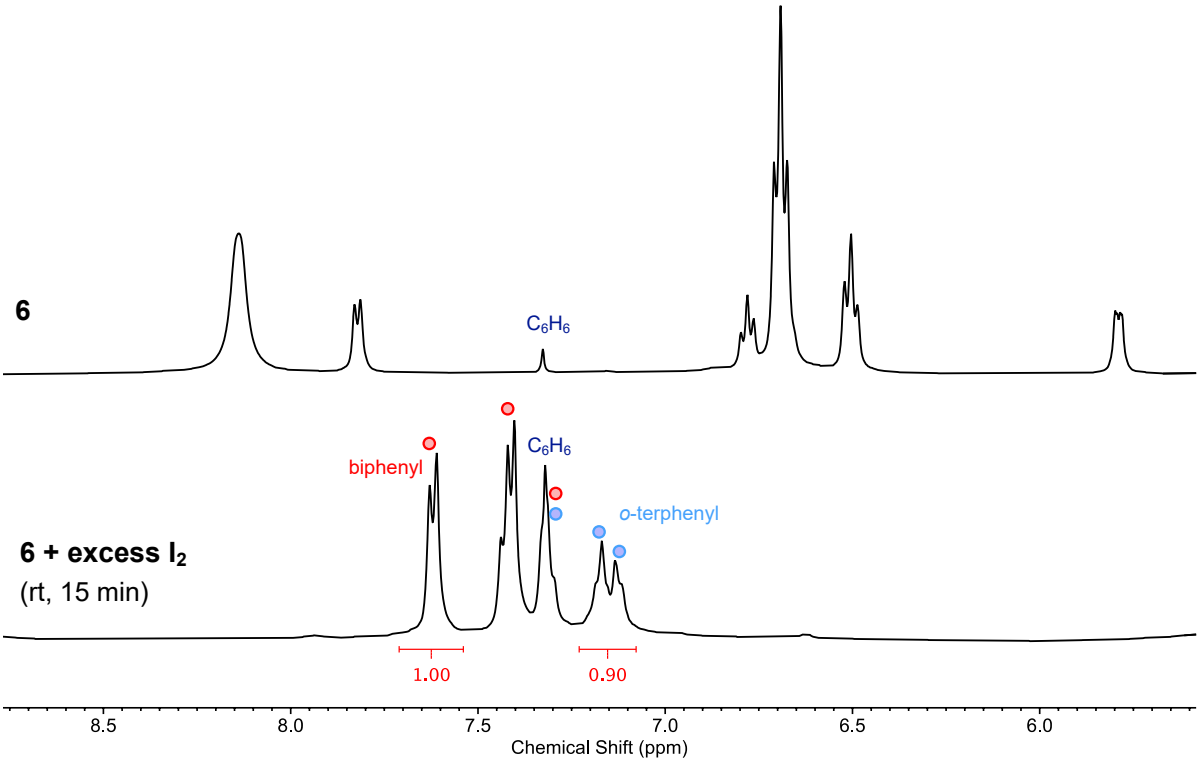

Figure S15: Reaction of **6** with excess I_2. Top: ^{1}H NMR of **6**; bottom: after room temperature addition of I_2.

MeI

^{1}H NMR clearly showed the formation of biphenyl and toluene (δ_H = 2.30 ppm). Remaining phenyl groups found as C_6H_6.

GC–MS allowed us to assign the small singlet at δ_H = 2.22 ppm to methyl-biphenyl derived from the C_6H_4 moiety (conversion of this moiety to methyl-biphenyl estimated to be 45% by ^{1}H NMR). We did not detect *o*-xylene, and the aromatic NMR signals of toluene, methyl-biphenyl, *o*-terphenyl overlap at 7.0–7.3 ppm precluding analysis of o-terphenyl yield. Biphenyl/toluene/Me-biphenyl ratio of approximately 2:2:1.

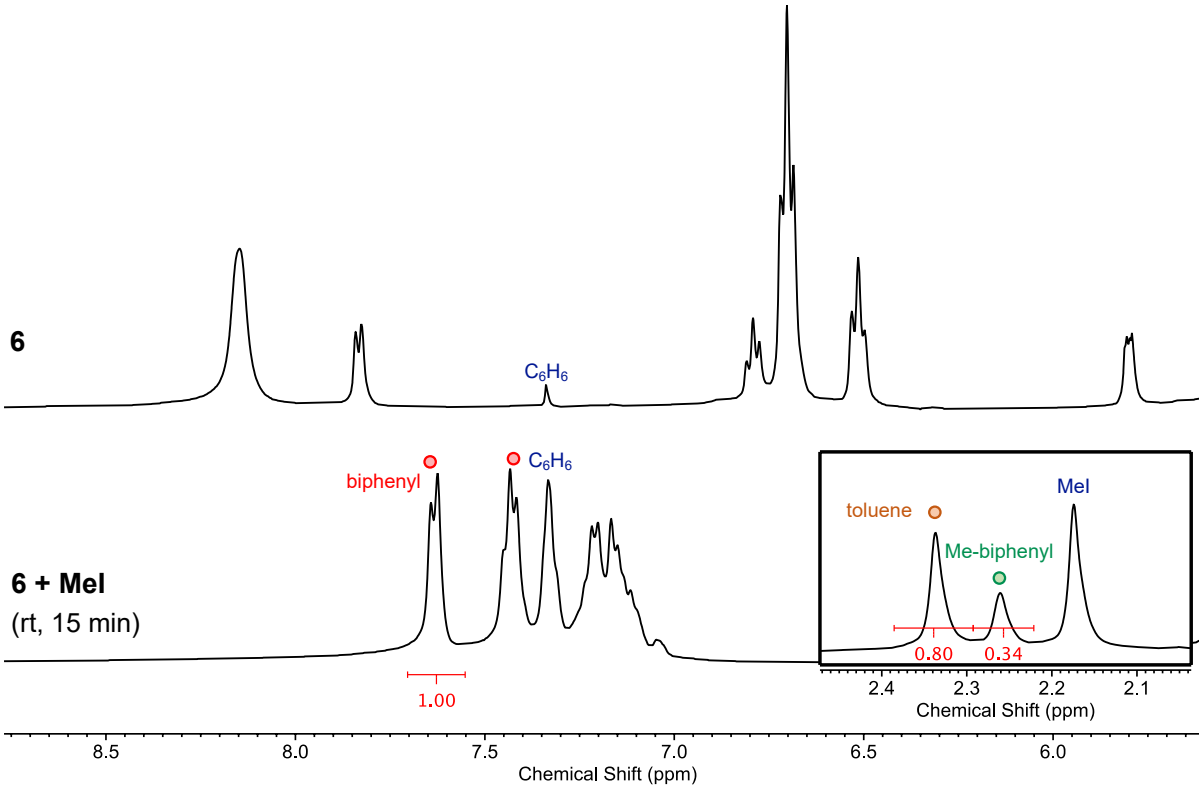

Figure S16: Reaction of **6** with ca. 4 equiv MeI. Top: ^{1}H NMR of **6**; bottom: after room temperature addition of MeI. Inset – Ar-CH_3 region.

Anthracene

Upon addition of 3 equiv anthracene to a THF-d_8 solution of **5**, a very deep blue solution was obtained. The signals of anthracene disappeared as judged by ^{1}H NMR spectroscopy, but the distinctive singlet of the triptycene bridgehead proton at 5–6 ppm was absent. Triptycene (254.3 g mol^{-1}) was not observed by GC–MS. Crystals of $Li_2(THF)_4NiPh_4$ were isolated from the reaction mixture.

Analysis of the reaction mixture after 70 h at rt showed that a set of signals from presumably a Ni complex disappeared. This confirmed that instead of cycloaddition reactivity, other reactions occur.

In the case of 1 equivalent of anthracene, complex **5** persists for longer.

Unfortunately, we were not able to crystallise the products of these reactions.

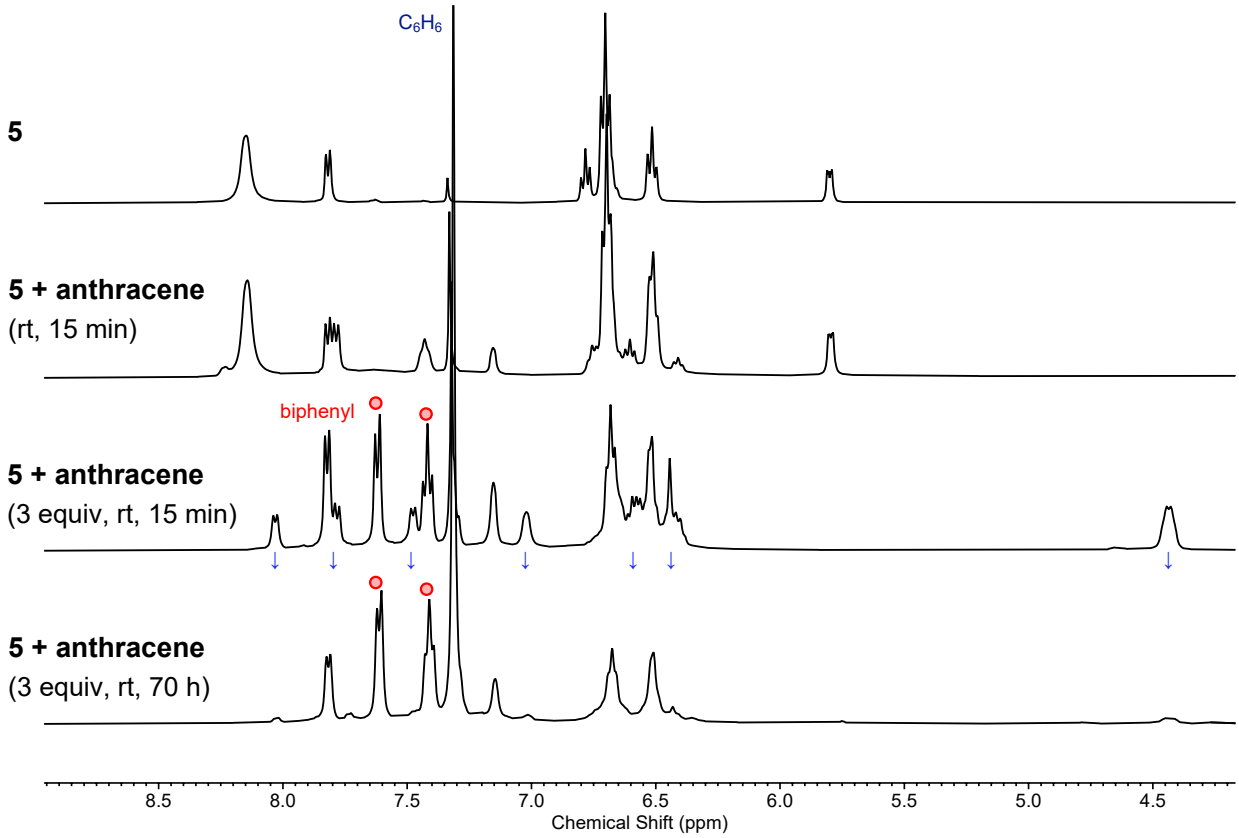

Figure S17: Reactions of **5** with anthracene. THF-d_8

Experiments with PhLi-$^{13}C_6$

Complex **4** (5.9 mg, 0.044 mmol, 1 equiv) and PhLi-$^{13}C_6$ (1.13 mg, ca. 3 equiv) were dissolved in **THF-d_8** (0.45 mL) at room temperature. The spectra displayed below in **Figure S18** show the initial appearance of the ^{13}C label in the PhLi ligands of the Ni(PhLi)$_2$ fragment (highlighted in blue at 142.9 ppm). After heating at 33 °C, very little change to the $^{13}C\{^1H\}$ NMR spectrum is observed. The reaction to form **2** does not proceed appreciably in THF.

Complex **4** (3.3 mg, 0.0025 mmol, 1 equiv) and PhLi-$^{13}C_6$ (0.9 mg, contains some LiBr, ca. 3 equiv) were dissolved in **Et_2O** (0.5 mL) at room temperature. The spectra displayed in **Figure S19** show the initial appearance of the ^{13}C label in the PhLi ligands of the Ni(PhLi)$_2$ fragment, and, after heating at 33 °C, the appearance of the ^{13}C label in the benzyne/type ligand (δ_C = 112 ppm, dd, 40 Hz, 17 Hz).

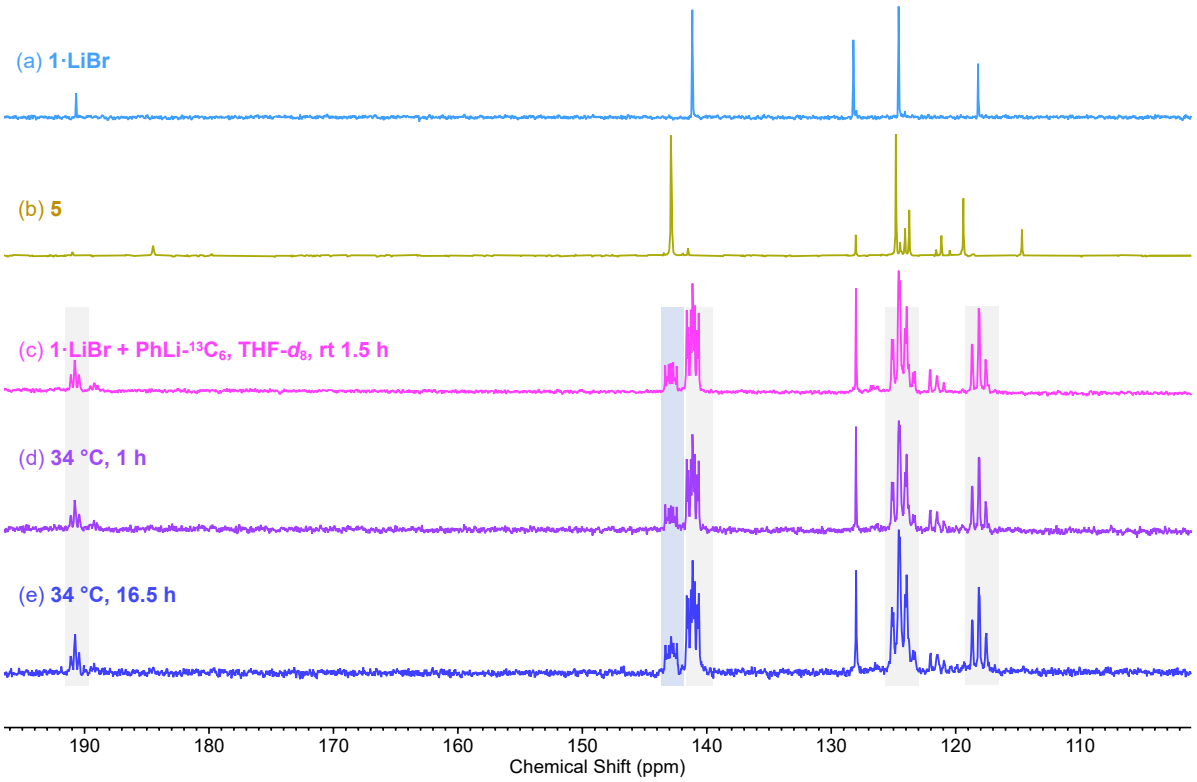

Figure S18. $^{13}C\{^1H\}$ NMR (100 MHz, 25 °C, THF-d_8) spectra.
(a) Complex **4** (natural abundance). (b): Complex **5** (natural abundance). (c) **4** + PhLi-$^{13}C_6$, rt, 90 min; (d) heated at 34 °C for 1 h; (e) heated at 34 °C for 16.5 h. PhLi-$^{13}C_6$ shaded in grey at 190.8, 141.2, 124.6, and 118.2 ppm.

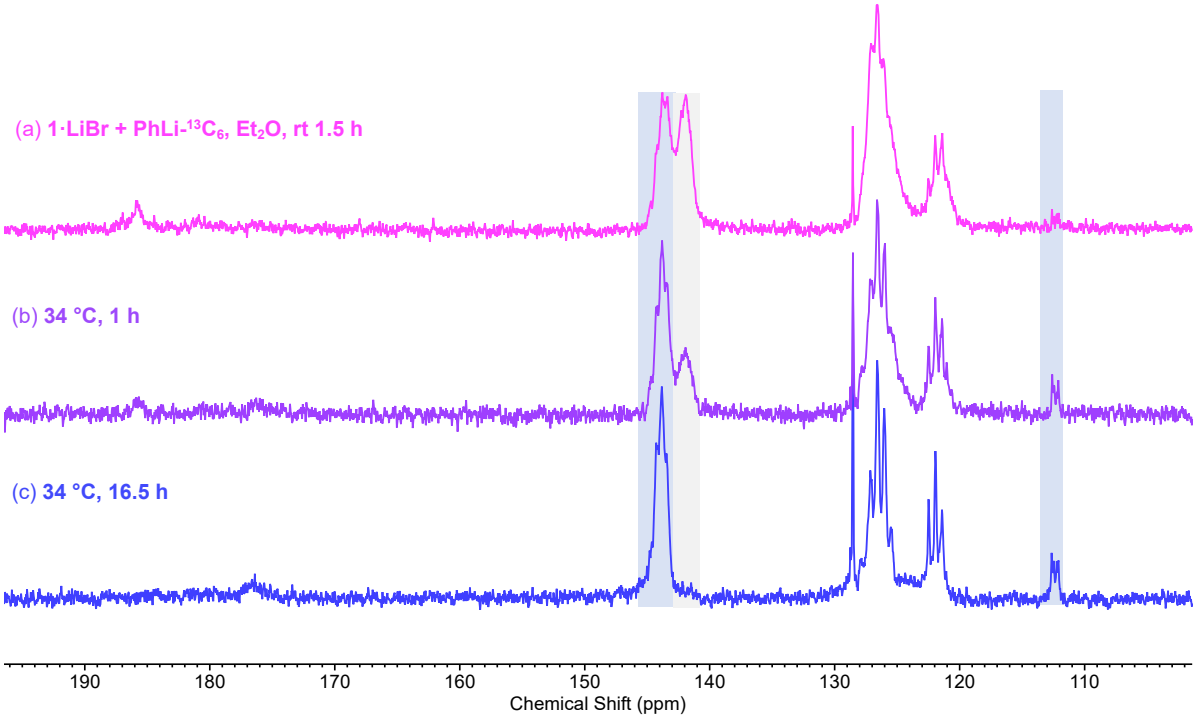

Figure S19. $^{13}C\{^1H\}$ NMR (100 Hz, 25 °C, Et_2O) spectra. (a) **4** + PhLi-$^{13}C_6$, rt, 90 min; (b) 34 °C for 1 h; (c) 34 °C for 16.5 h. PhLi-$^{13}C_6$ shaded in grey at 141.2 ppm.

Catalysis

Csp^2-Csp^3 Kumada-Tamao-Corriu coupling

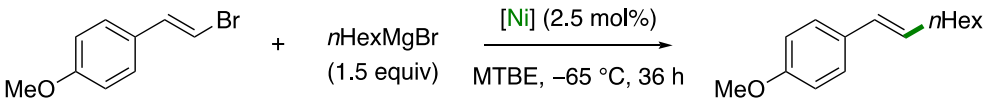

General procedure:[11]

An ampoule containing a 0.2 M MTBE solution of (*E*)-(2-bromovinyl)benzene (36.6 mg, 0.2 mmol, 1 equiv) and *n*-hexylMgBr (2 M in Et_2O, 150 µL, 0.3 mmol, 1.5 equiv) was cooled to −65 °C. In a separate ampoule, the Ni complex (0.005 mmol, 0.025 equiv) was dissolved in MTBE (100 µL). The resulting red solution was added to the reaction mixture at −65 °C and this temperature maintained for 36 h. After this time, the reaction was allowed to warm to room temperature, quenched with 3 mL water, then extracted with EtOAc. Purification by column chromatography (silica, hexane) gave the desired cross-coupled product (*E*)-1-phenyl-1-octene. Spectral data matched literature values.[12]

Isolated yields of (*E*)-1-phenyl-1-octene:
Catalyst **2**: 74%
Catalyst **5**: 43%

Buchwald-Hartwig amination

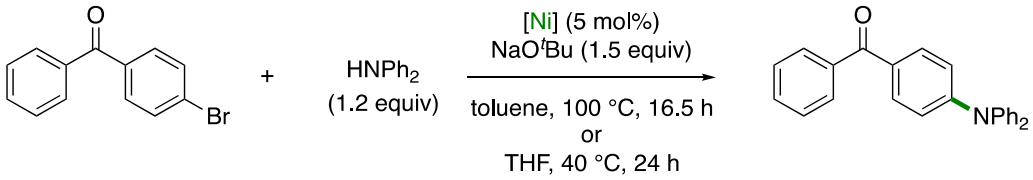

General procedure:

The reaction was carried out following literature procedures:[13,14]

Diphenylamine (50.8 mg, 0.30 mmol, 1.2 equiv) and 4-bromobenzophenone (65.3 mg, 0.25 mmol, 1 equiv) were weighed into an ampoule. In the glovebox, the Ni complex (0.00625 mmol, 0.025 equiv), NaO^{t}Bu (36 mg, 0.375 mmol, 1.5 equiv) were added as solids followed by 0.2 mL solvent. The resulting dark reaction mixture was transferred to a preheated oil bath at 100 °C (toluene, 16.5 h) or 40 °C (THF, 24 h). After this time, the brown-red reaction mixture was quenched with 8 mL water and extracted with CH_2Cl_2 (20 mL total). After drying with $MgSO_4$, purification by column chromatography (silica, hexane/EtOAc 100:4) gave the desired product as a bright yellow solid.

Isolated yields (toluene, 100 °C, 16.5 h):
Catalyst **2**: 34 mg, 28%.
Catalyst **5**: 19.3 mg, 22%.
[$Ni(COD)_2$]: 46 mg, 54%.
Isolated yields (THF, 40 °C, 24 h):
Catalyst **2**: 8 mg, 9%.
Catalyst **5**: 5.6 mg, 6.5%.

Coupling of 2-methoxynaphthalene with PhLi

2-Methoxynaphthalene (31.7 mg, 0.20 mmol), $PhLi(THF)_{0.95}$ (33.5 mg, 0.22 mmol, 1.1 equivalents) and tetramethylsilane (7 µL, 0.05 mmol, 25 mol%) were dissolved in 500 µL of C_6D_6. The ^1H NMR spectrum was run to determine the ratio of 2-methoxynaphthalene with respect to the internal standard. The catalyst (compound **2** or **5**, 0.005 mmol, 2.5 mol%) was added and the ^1H NMR spectrum was recorded immediately and then periodically whilst the samples remained at room temperature (25 °C). The consumption of starting materials and the cross-coupled product (2-phenylnaphthalene) were determined against the internal standard.

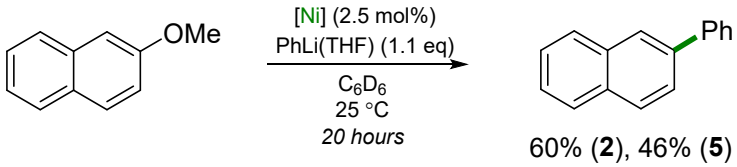

60% (**2**), 46% (**5**)

NMR yields (C_6D_6, 25 °C, 20 h):
Catalyst **2**: 60%.
Catalyst **5**: 46%.

Reactivity of intermediate nickelates with N_2

During studies towards the synthesis of "$Li_3NiPh_3(THF)_3$" we carried out two reactions where we employed Ni(CDT) as an alternative source of Ni(0) in reactions with excess PhLi.

One NMR-scale reaction was carried out between Ni(CDT) (5.9 mg, 0.027 mmol) and PhLi (6.7 mg, 0.080 mmol, 3 equiv) in 0.5 mL THF-d_8 in a N_2-filled glovebox. Slow evaporation of deep red THF/pentane solution at −35 °C resulted in small rhombic red crystals that were identified as a previously reported complex with N_2 ligands bridged side-on to the two Ni atoms.[15,16]

A second reaction was carried out on a larger scale [15 mg Ni(CDT)] and taken to dryness. Single crystals were grown by slow evaporation of an ether solution of the residue, and under the microscope a number of different shapes/colours of crystal were visible. One was found to be $Li_2NiPh_4(THF)_4$, and another a complex with a similar dinickel dinitrogen core to that described above but containing a cube of Li atoms with the faces capped with OEt or N atoms (see **Figure S22**). A very similar complex was reported by Jonas and co-workers.[17] In that case, the cube was made of Na atoms due to the mixture of PhLi and PhNa employed in their reaction with Ni(CDT).

These reactions confirmed the requirement for all syntheses of nickelates described herein to be carried out under argon.

X-ray Crystallography

The crystal structures of all new compounds have been deposited into the Cambridge Crystallographic Data Centre (CCDC) and have been assigned the following numbers: 2127441 (**4**), 2127442 (**5**), 2127151 (**6**), 2127152 (**7**), 2127153 (**8**) and 2127443 (N_2-Complex). Selected crystallographic and refinement parameters are presented below (**Table S1** and **Table S2**).

Complexes 4, 5, and N_2-Complex

Single crystals of suitable size, coated with dry perfluoropolyether or oil were mounted on a glass fiber and fixed in a cold nitrogen stream [T = 193 K] to the goniometer head. Data collection was performed on a Bruker D8 Quest APEX-III CCD area detector Photon III using monochromatic radiation λ (Mo Kα1) = 0.71073 Å by a Iμs 3.0 microfocus X-ray source. Data collections were processed with APEX-W2D-NT (Bruker, 2004), cell refinement and data reduction with SAINT-Plus (Bruker, 2004) and the absorption was corrected by multiscan method applied by SADABS. The space-group assignment was based upon systematic absences, E statistics, and successful refinement of the structure. The structure was solved by direct methods and expanded through successive difference Fourier maps, F2 (SHELXTL). In the last cycles of refinement, ordered non-hydrogen atoms were refined anisotropically. Hydrogen atoms connected to carbon atoms were included in idealized positions, and a riding model was used for their refinement, except for: H58 and H55 (in complex **5**), H18 and H13 (in complex 1) and H18, H17, H13, H14, H77, H78, H81 and H82 (in complex **4**) that were located in the Fourier map and freely refined.

Complexes 6, 7, and 8

In all cases, crystals were immersed in an inert parabar oil, mounted at ambient conditions, and transferred into the nitrogen stream (100 or 173 K).

Measurements were made on a *RIGAKU Synergy S* area-detector diffractometer using mirror optics monochromated Cu Kα radiation (λ = 1.54184 Å). Data reduction was performed using the *CrysAlisPro* program.[18] The intensities were corrected for Lorentz and polarization effects, and an absorption correction based on the Gaussian method using SCALE3 ABSPACK in *CrysAlisPro* was applied. The structure was solved by direct methods or intrinsic phasing using *SHELXT*,[19] which revealed the positions of all non-hydrogen atoms of the compounds. All non-hydrogen atoms were refined anisotropically. H-atoms were assigned in geometrically calculated positions and refined using a riding model where each H-atom was assigned a fixed isotropic displacement parameter with a value equal to 1.2Ueq of its parent atom (1.5Ueq for methyl groups). Refinement of the structure was carried out on F^2 using full-matrix least-squares procedures, which minimized the function $\Sigma w(F_o^2 - F_c^2)^2$. The weighting scheme was based on counting statistics and included a factor to downweight the intense reflections. All calculations were performed using the *SHELXL-2014/7*[20] program in OLEX2.[21]

For $Li_5(solv)_5Ph_5Ni_2(C_6H_4)$ (**6**), substitutional disorder was modelled for parts of the molecule where three lithium coordination sites can be occupied either by THF or Et_2O. The occupancies of each disorder component were refined by the use of a free variable. The sum of equivalent components was

constrained to 1 *i.e.* 100%. For $[Na_2(THF)_3Ph_2NiCOD]_2$ (**7**), disorder models were used for one of the independent half units where the occupancies of each disorder component were refined through the use of free variables. For $[Na_2(Et_2O)_3Ph_2(NaC_8H_{11})NiCOD]_2$ (**8**), a disorder model was used where the disordered part was split into two components, the occupancies of each component was refined through the use of a free variable. The sum of both components was constrained to 100%.

	4	**5**	**N_2-Complex**
Formula	$C_{128}H_{224}Br_4Li_{12}Ni_4O_{16}$	$C_{58}H_{73}Li_6Ni_2O_4$	$C_{88}H_{124}Li_{12}N_4Ni_4O_{12}$
fw	2656.72	993.22	1747.95
Crystal size, mm	0.25x0.2x0.1	0.25x0.21x0.19	0.1x012x0.29
Crystal system	monoclinic	triclinic	monoclinic
Space group	P 1 21/c 1	P -1	P 1 21/c 1
a, Å	18.6770(8)	13.1760(12)	19.0297(12)
b, Å	19.8681(7)	14.1453(12)	12.2915(8)
c, Å	39.5750(16)	15.9321(15)	21.1653(13)
α, deg	90	101.573(3)	90
β, deg	91.001(2)	103.502(4)	110.588(2)
γ, deg	90	101.439(3)	90
V, $Å^3$	14683.1	2733.3(4)	4634.5(5)
T, K	193.0	193.0	193.0
Z	4	2	2
ρcalc, $g \cdot cm^{-3}$	1.202	1.207	1.253
μ, mm^{-1} (Mo1Kα)	1.646	0.731	0.857
F (000)	5632.0	1054	1848
Absoption correction	multi-scan 0.5715-0.7453	multi-scan 0.6444-0.7454	multi-scan 0.6948-0.7457
θ range, deg	27.123-2.050	1.361-26.511	1.950-25.250
No. of rflns measd	32337	11282	8389
Rint	0.0513	0.1139	0.1243
No. of rlfns unique	32337	11282	8389
No. of params/restraints	1533/98	645/24	543/93
R1 (I > 2σ(I))	0.0675	0.0624	0.0659
R1 (all data)	0.1060	0.1336	0.1210
wR2 (I > 2σ(I))	0.1755	0.1437	0.1568
wR2 (all data)	0.1962	0.1806	0.2037
Diff. Fourier peaks min/max, $eÅ^{-3}$	-1.210/1.977	-0.714/1.283	-0.810/0.738
CCDC number	2127441	2127442	2127443

Table S1: Crystal data and structure refinement details for compounds **4**, **5**, and **N_2-Complex**.

Compound	**6**	**7**	**8**
Identification code	21EH168_AMB-609	21EH072_AMB-438	21EH115_AMB-502
Empirical formula	$C_{56}H_{71.75}Li_5Ni_2O_5$	$C_{64}H_{92}Na_4Ni_2O_6$	$C_{80}H_{126}Na_6Ni_2O_6$
Formula weight	977	1166.75	719.58
Temperature/K	173.01(10)	100.00(10)	100.01(10)
Crystal system	monoclinic	triclinic	monoclinic
Space group	$P2_1/c$	P-1	C2/c
a/Å	16.24036(9)	11.66550(10)	21.45144(13)
b/Å	14.66026(7)	12.7905(2)	17.82545(10)
c/Å	22.76116(11)	22.7870(2)	22.25202(14)
α/°	90	104.1210(10)	90
β/°	101.7134(5)	90.4700(10)	109.7306(7)
γ/°	90	109.7120(10)	90
Volume/Å^3	5306.30(5)	3088.75(7)	8009.21(9)
Z	4	2	4
ρ_{calc}g/cm^3	1.223	1.255	1.194
μ/mm^{-1}	1.217	1.406	1.271
F(000)	2075	1248	3104
Crystal size/mm^3	0.243 × 0.092 × 0.071	0.209 × 0.18 × 0.116	0.225 × 0.205 × 0.135
Radiation	Cu Kα (λ = 1.54184)	Cu Kα (λ = 1.54184)	Cu Kα (λ = 1.54184)
2Θ range for data collection/°	5.558 to 138.274	7.608 to 131.058	6.614 to 146.996
Index ranges	-19 ≤ h ≤ 19, -17 ≤ k ≤ 17, -24 ≤ l ≤ 27	-13 ≤ h ≤ 13, -15 ≤ k ≤ 13, -26 ≤ l ≤ 26	-26 ≤ h ≤ 26, -22 ≤ k ≤ 22, -27 ≤ l ≤ 27
Reflections collected	102036	112942	113505
Independent reflections	9893 [R_{int} = 0.0450, R_{sigma} = 0.0219]	10643 [R_{int} = 0.0389, R_{sigma} = 0.0161]	8086 [R_{int} = 0.0467, R_{sigma} = 0.0155]
Data/restraints/parameters	9893/100/757	10643/140/1068	8086/17/524
Goodness-of-fit on F^2	1.035	1.034	1.057
Final R indexes [I>=2σ (I)]	R_1 = 0.0410, wR_2 = 0.1167	R_1 = 0.0398, wR_2 = 0.1026	R_1 = 0.0494, wR_2 = 0.1357
Final R indexes [all data]	R_1 = 0.0443, wR_2 = 0.1203	R_1 = 0.0424, wR_2 = 0.1044	R_1 = 0.0509, wR_2 = 0.1369
Largest diff. peak/hole / e Å^{-3}	0.64/-0.48	0.44/-0.34	0.66/-0.53
CCDC number	2127151	2127152	2127153

Table S2: Crystal data and structure refinement details for compounds **6**–**8**.

Molecular Structure of 4

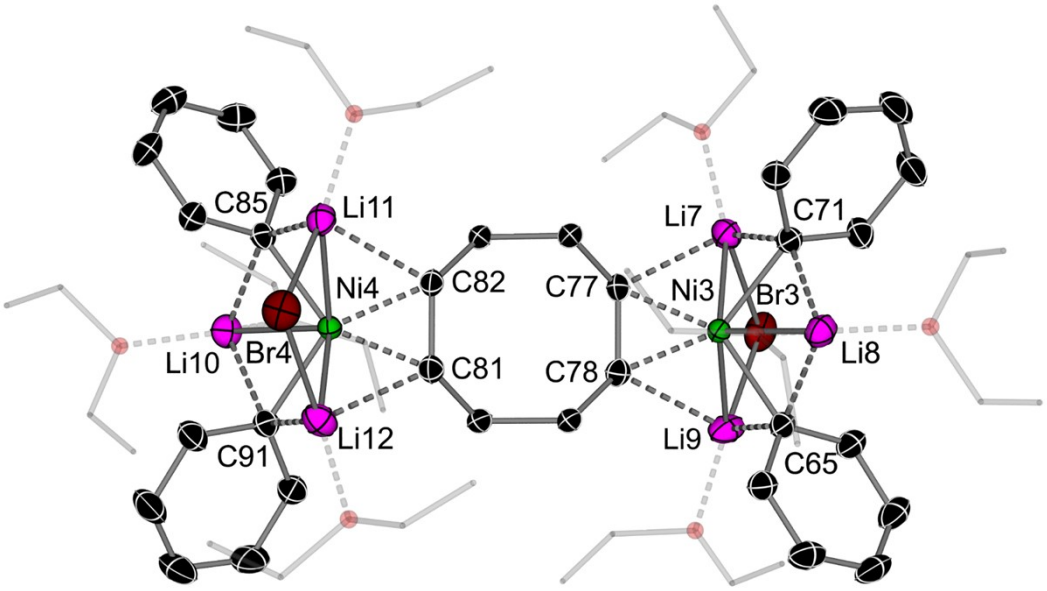

Figure S20: Molecular structure of **4**. Thermal ellipsoids shown at 30% probability. Hydrogen atoms omitted for clarity. Only one of two independent molecules in the asymmetric unit is shown.

C81–C82	1.450(6)	Li12–C91	2.38(1)
C77–C78	1.451(6)	Li7–C71	2.37(1)
Ni4–C81	1.962(4)	Li7–C77	2.37(1)
Ni4–C82	1.969(4)	Li8–C65	2.323(9)
Ni3–C77	1.980(4)	Li8–C71	2.322(9)
Ni3–C78	1.952(4)	Li9–C65	2.33(1)
Ni4–C85	1.965(4)	Li9–C78	2.40(1)
Ni4–C91	1.972(4)	Li11–Br4	2.489(9)
Ni3–C65	1.961(4)	Li12–Br4	2.506(9)
Ni3–C71	1.968(4)	Li7–Br3	2.483(9)
Ni4–Li10	2.649(8)	Li9–Br3	2.51(1)
Ni4–Li11	2.451(8)	C85–Ni4–C82	105.4(2)
Ni4–Li12	2.463(9)	C85–Ni4–C91	107.8(2)
Ni3–Li7	2.448(9)	C91–Ni4–C81	103.5(2)
Ni3–Li8	2.610(8)	C81–Ni4–C82	43.3(2)
Ni3–Li9	2.43(1)	Li11–Br4–Li12	84.1(3)
Li10–C85	2.323(9)	C65–Ni3–C78	104.3(2)
Li10–C91	2.400(9)	C65–Ni3–C71	105.6(2)
Li11–C82	2.38(1)	C71–Ni3–C77	106.7(2)
Li11–C85	2.320(9)	C77–Ni3–C78	43.3(2)
Li12–C81	2.41(1)	Li7–Br3–Li9	84.5(3)

Table S3: Selected bond lengths [Å] and angles [°] in **4**.

Molecular Structure of 5

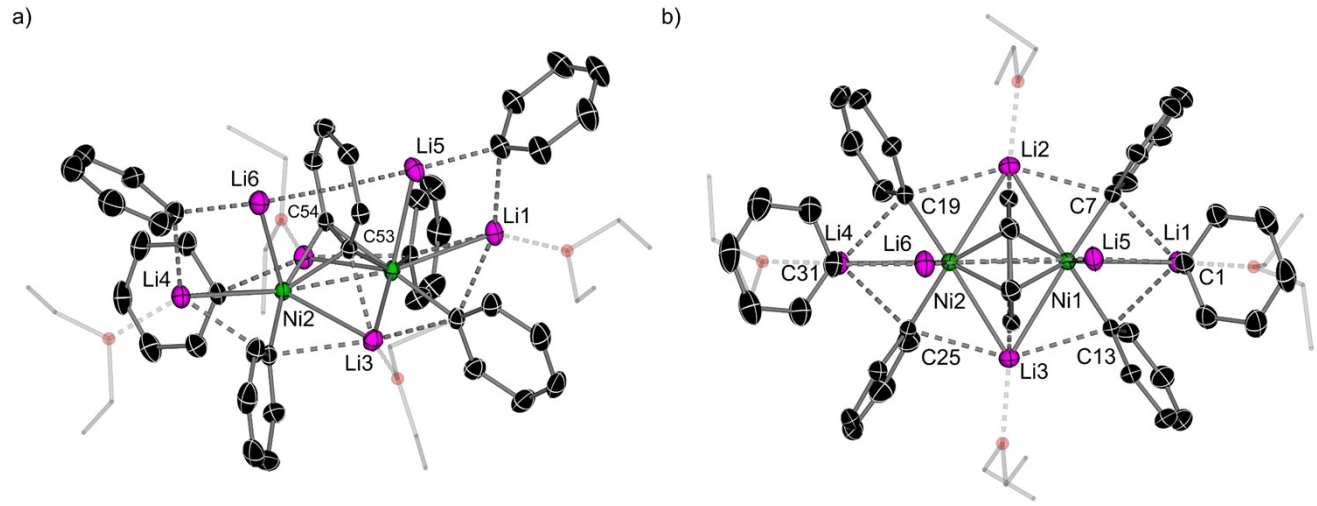

Figure S21: Molecular structure of **5**. Thermal ellipsoids shown at 30% probability. Hydrogen atoms omitted for clarity. a) Side view. b) Top-down view.

Ni2–Ni1	2.7117(8)	C19–Li4	2.40(1)
Ni2–Li6	2.55(1)	Ni2–C54	1.925(3)
Li6–C31	2.09(1)	Ni2–C53	1.937(4)
C31–Li4	2.24(1)	C54–C53	1.449(6)
Li4–Ni2	2.564(9)	C53–Ni1	1.938(5)
Li4–C25	2.36(1)	Ni1–C54	1.945(5)
C25–Ni2	1.945(5)	C53–C54	1.449(6)
Ni2–Li3	2.65(1)	C53–C58	1.427(7)
Li3–C25	2.51(1)	C58–C57	1.385(7)
Li3–Ni1	2.610(9)	C57–C56	1.416(8)
Ni1–C13	1.955(6)	C55–C54	1.422(7)
C13–Li3	2.44(1)	C55–C56	1.391(7)
Ni1–Li1	2.560(8)	C57–C58	1.385(7)
Li1–C13	2.40(1)	C56–C55	1.391(7)
Li1–C7	2.447(9)	Li6–centroid	1.968
C7–Ni1	1.944(6)	Li5–centroid	1.958
Li2–C7	2.462(9)	Ni1–C7–Li1	70.2(3)
Ni1–Li2	2.664(9)	C7–Li1–Ni1	45.6(2)
Li2–Ni2	2.65(1)	Li1–Ni1–C7	64.1(2)
Ni2–C19	1.940(4)	Ni1–Li1–C1	103.4(4)
C19–Li2	2.457(9)	Li1–C1–Li5	80.9(4)

Table S4: Selected bond lengths [Å] and angles [°] in **5**.

Molecular Structure of N_2-Complex

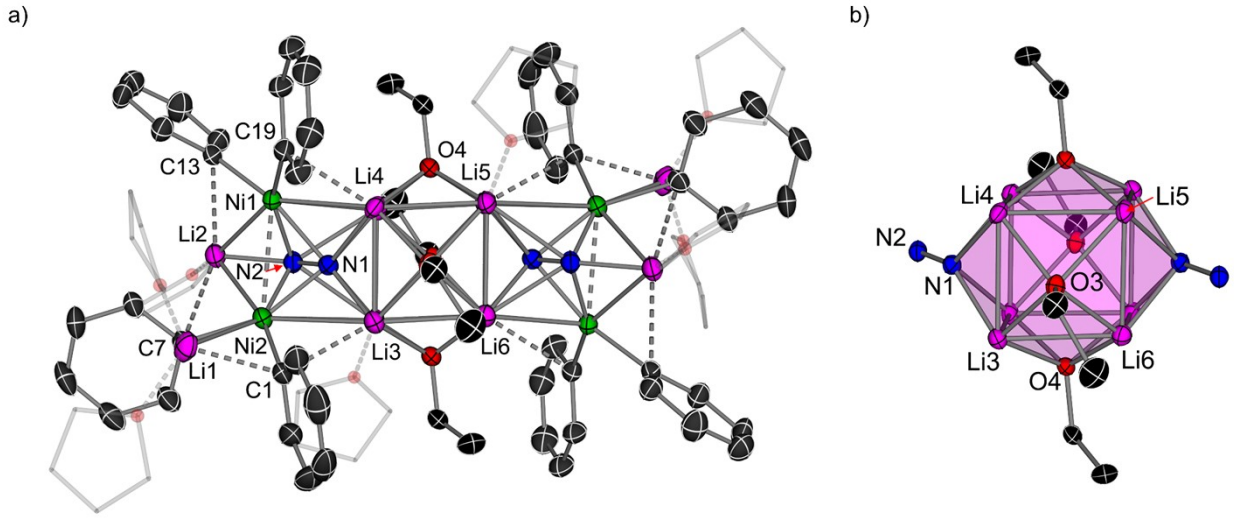

Figure S22: a) Full molecular structure of **N_2-Complex**. Thermal ellipsoids shown at 30% probability. Hydrogen atoms omitted for clarity. b) Simplified view of the internal tetrakis-hexahedron.

Ni1–Ni2	2.679(1)	Ni1–Li2	2.59(1)
Ni1–C19	1.931(7)	Ni1–Li4	2.590(9)
Ni1–C13	1.940(5)	Ni2–Li1	2.548(9)
Ni2–C1	1.953(6)	Ni2–Li2	2.65(1)
Ni2–C7	1.961(6)	O3–Li6	1.954(8)
N1–N2	1.365(6)	O3–Li5	2.04(1)
Ni1–N1	1.892(4)	O3–Li4	1.955(9)
Ni1–N2	1.943(4)	O3–Li3	1.99(1)
Ni2–N1	1.930(4)	O4–Li6	1.95(1)
Ni2–N2	1.912(4)	O4–Li5	2.20(1)
Li1–C7	2.35(1)	O4–Li4	1.969(9)
Li1–C1	2.25(1)	O4–Li3	1.962(8)
Li2–C13	2.47(1)	C13–Ni1–C19	100.8(2)
Li2–C7	2.53(1)	C7–Ni2–C1	104.0(2)
Li2–N2	1.91(1)	N1–Ni1–C19	111.3(2)
Li3–C1	2.39(1)	N1–Ni2–C1	106.2(2)
Li3–N1	1.997(9)	N2–Ni1–C13	106.0(2)
Li4–C19	2.409(9)	N2–Ni2–C7	109.3(2)
Li4–N1	2.08(1)	N1–Ni1–N2	41.7(2)
Li5–N1	2.210(9)	Ni–Ni2–N2	41.6(2)
Li6–N1	2.071(9)		

Table S5: Selected bond lengths [Å] and angles [°] in **N_2-Complex**.

Molecular Structure of 6

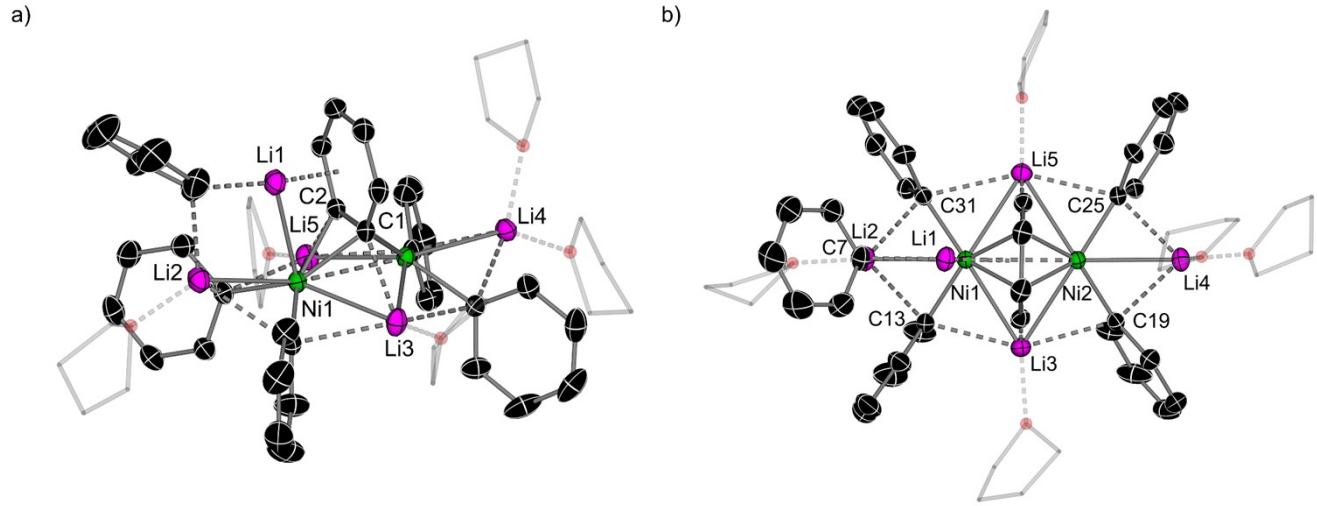

Figure S23: Molecular structure of **6**. Thermal ellipsoids shown at 30% probability. Hydrogen atoms omitted for clarity. a) Side view. b) Top-down view.

C1–C2	1.436(3)	Li2–C7	2.221(4)
Ni1–C1	1.951(1)	Li3–C19	2.437(3)
Ni1–C2	1.958(2)	Li3–C13	2.426(4)
Ni2–C1	1.954(2)	Li3–C1	2.197(4)
Ni2–C2	1.945(2)	Li4–C25	2.310(4)
Ni1–Ni2	2.7308(4)	Li4–C19	2.386(4)
Ni1–C13	1.968(2)	Li5–C31	2.479(3)
Ni1–C31	1.970(2)	Li5–C25	2.426(3)
Ni2–C19	1.956(2)	Li5–C2	2.193(3)
Ni2–C25	1.965(2)	Li1–centroid	1.871
Ni1–Li3	2.583(3)	C13–Ni1–C31	103.95(8)
Ni1–Li5	2.561(3)	C19–Ni2–C25	103.52(8)
Ni1–Li2	2.533(3)	C13–Ni1–Ni2	120.04(6)
Ni1–Li1	2.552(3)	C31–Ni1–Ni2	122.28(5)
Ni2–Li5	2.569(3)	C25–Ni2–Ni1	120.17(6)
Ni2–Li4	2.538(3)	C19–Ni2–Ni1	119.01(6)
Ni2–Li3	2.592(3)	C1–Ni1–C2	43.09(7)
Li1–C7	2.102(4)	C1–Ni2–C2	43.21(7)
Li2–C31	2.405(4)	Li2–Ni2–Ni2	166.79(8)
Li2–C13	2.505(4)	Li4–Ni2–Ni1	177.71(8)

Table S6: Selected bond lengths [Å] and angles [°] in **6**.

Molecular Structure of 7

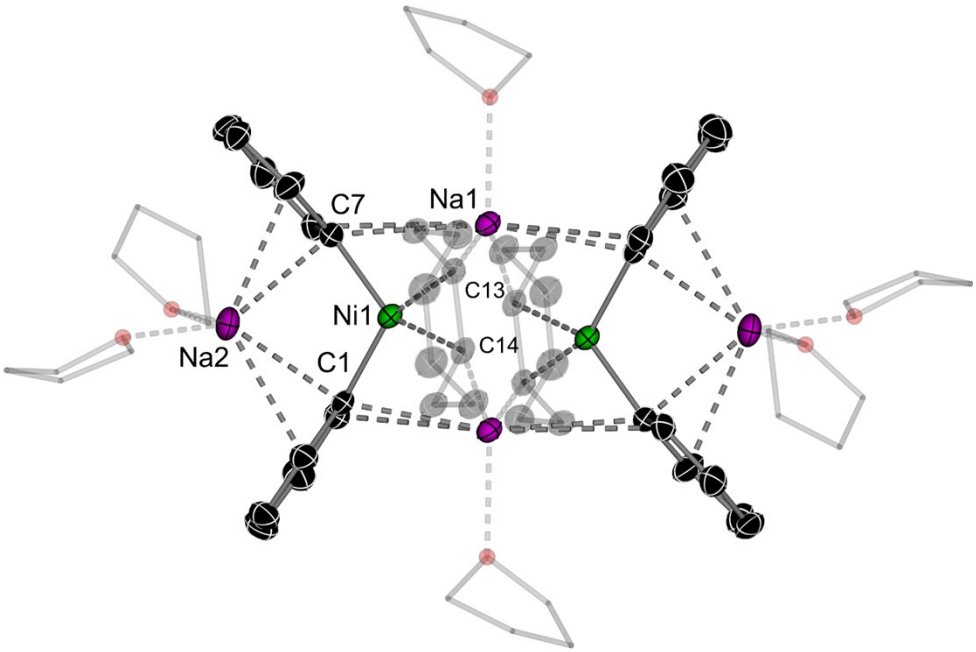

Figure S24: Molecular structure of **7**. Thermal ellipsoids shown at 30% probability. Hydrogen atoms omitted for clarity. Only one of two independent molecules in the asymmetric unit is shown.

Ni1–C1	1.963(2)	Na1–C13	2.941(3)
Ni1–C7	1.959(2)	C13–C14	1.447(3)
Ni1–C13	1.964(2)	Na1–C1	2.705(2)
Ni1–C14	1.960(2)	Na1–C14	2.794(2)
Ni1–Na1	2.7880(9)/2.9196(9)	C7–Ni1–C1	101.47(8)
Ni1–Na2	2.9371(8)	C13–Ni1–C7	105.96(8)
Na2–C1	2.603(2)	C14–Ni1–C1	108.71(8)
Na2–C7	2.545(2)	C14–Ni1–C13	43.28(8)
Na1–C7	2.888(2)		

Table S7: Selected bond lengths [Å] and angles [°] in **7**.

Molecular Structure of 8

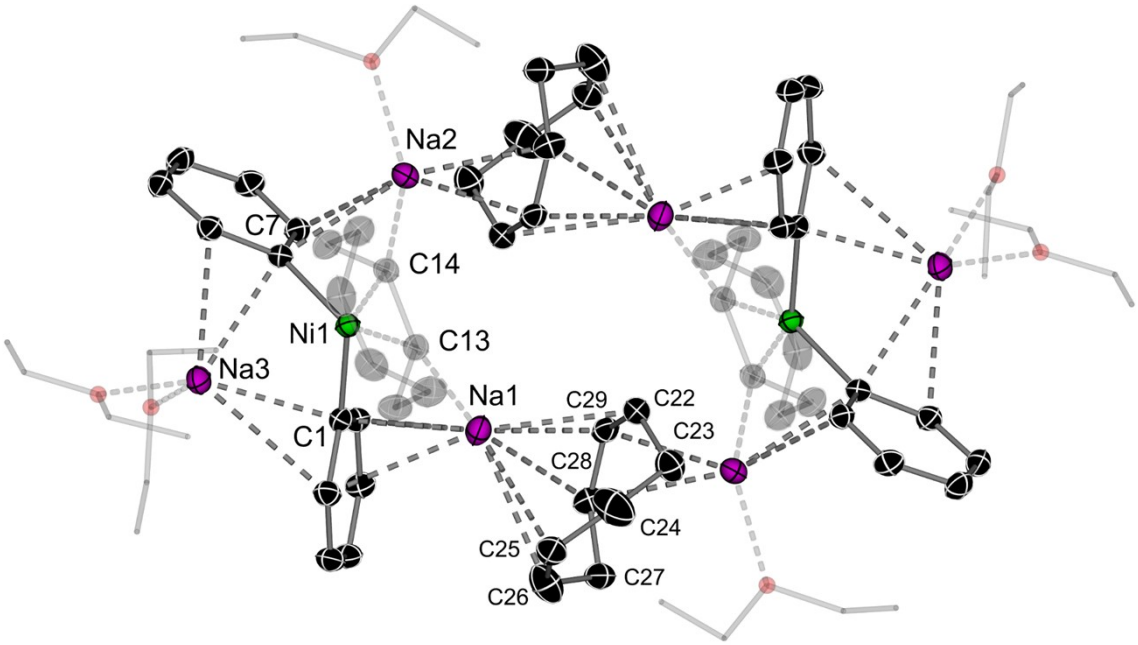

Figure S25: Molecular structure of **8**. Thermal ellipsoids shown at 30% probability. Hydrogen atoms omitted for clarity.

C13–C14	1.453(3)	Na2–C28	2.674(3)
Ni1–C1	1.968(2)	Na3–C7	2.617(3)
Ni1–C7	1.962(2)	Na3–C1	2.592(2)
Ni1–C13	1.972(2)	C22–C29	1.373(3)
Ni1–C14	1.959(2)	C23–C22	1.501(3)
Na1–C1	2.513(2)	C24–C23	1.523(5)
Na1–C13	2.674(2)	C25–C24	1.461(6)
Na1–C22	2.809(3)	C26–C25	1.343(4)
Na1–C29	2.506(3)	C27–C26	1.506(4)
Na1–C28	2.868(3)	C28–C27	1.514(3)
Na1–C26	2.952(3)	C29–C28	1.394(4)
Na1–C25	2.844(2)	C7–Ni1–C1	102.58(8)
Na2–C7	2.649(2)	C1–Ni1–C13	106.77(9)
Na2–C14	2.711(2)	C13–Ni1–C14	43.38(9)
Na2–C29	2.660(2)	C14–Ni1–C7	107.25(9)

Table S8: Selected bond lengths [Å] and angles [°] in **8**.

NMR Spectra of Reported Compounds

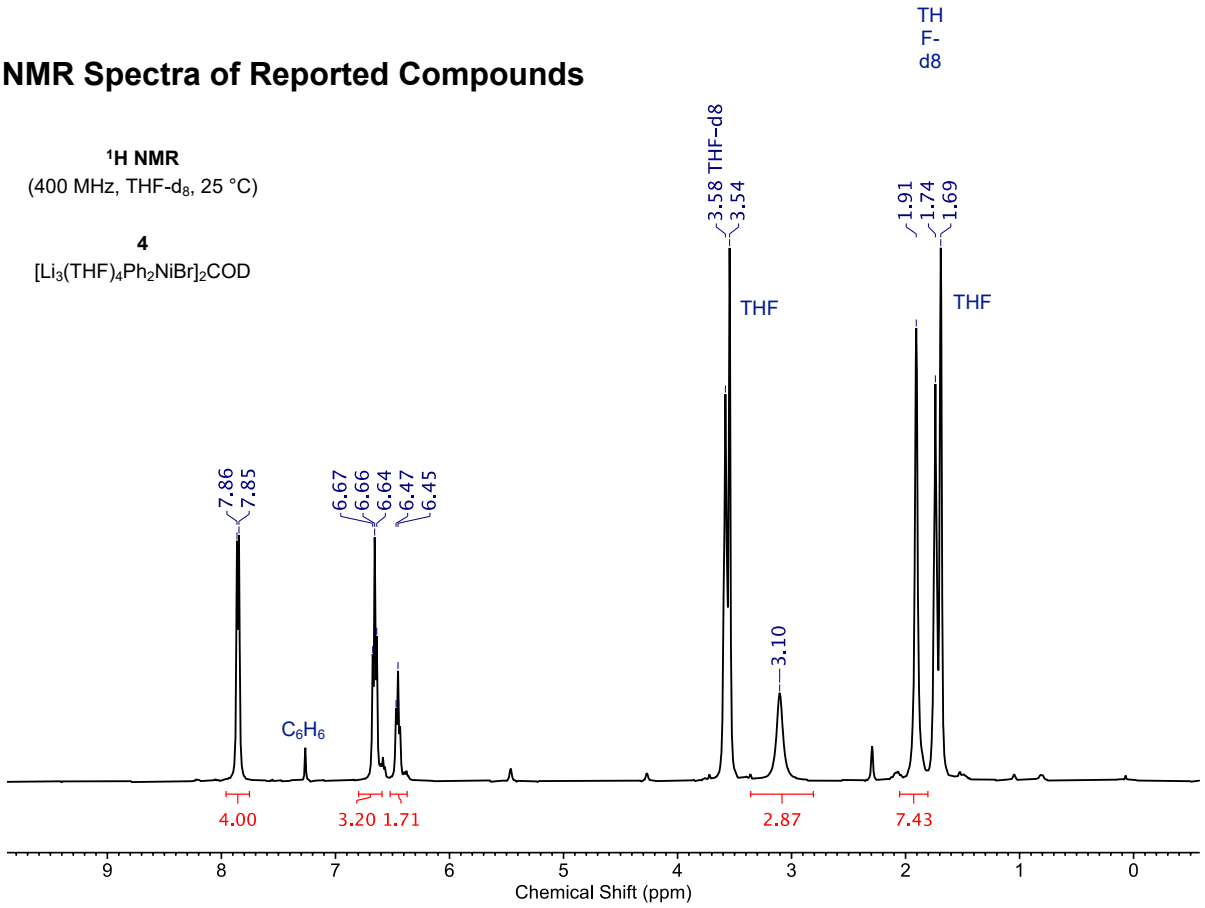

^{1}H NMR
(400 MHz, THF-d_8, 25 °C)

4
$[Li_3(THF)_4Ph_2NiBr]_2COD$

Spectrum S1: ^{1}H NMR spectrum of **4** in THF-d_8.

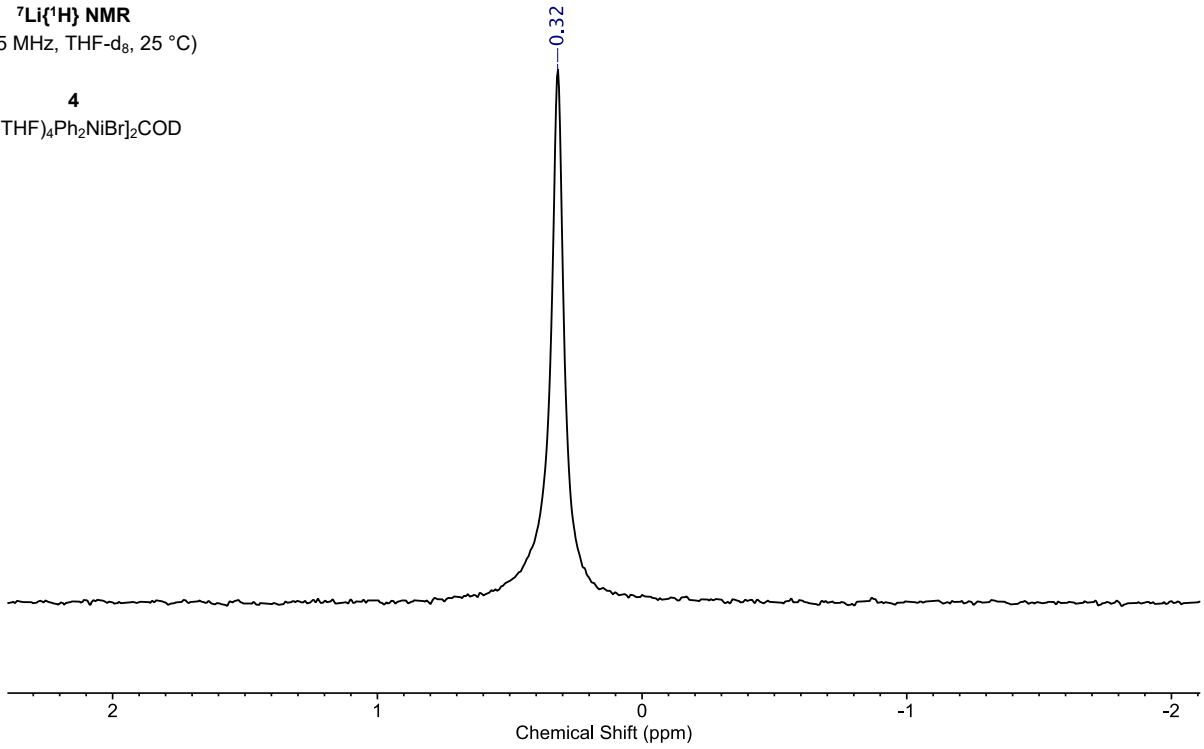

^{7}Li{^{1}H} NMR
(155.5 MHz, THF-d_8, 25 °C)

4
$[Li_3(THF)_4Ph_2NiBr]_2COD$

Spectrum S2: ^{7}Li{^{1}H} spectrum of **4** in THF-d_8. at 25 °C.

^{7}Li{^{1}H} NMR
(155.5 MHz, THF-d_8, 25 °C)

4
$[Li_3(THF)_4Ph_2NiBr]_2COD$

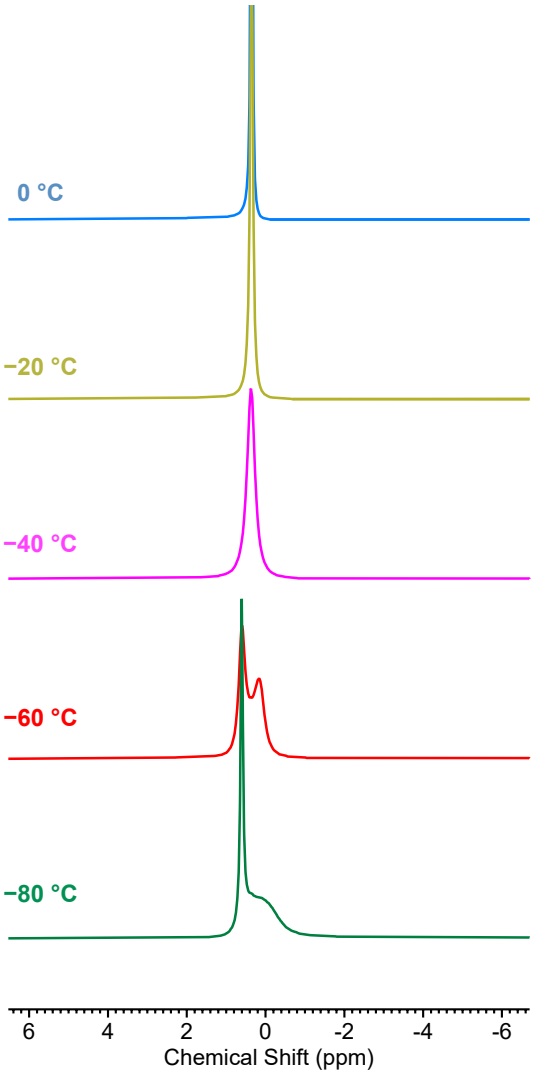

Spectrum S3: VT NMR (^{7}Li{^{1}H}) of **4**.

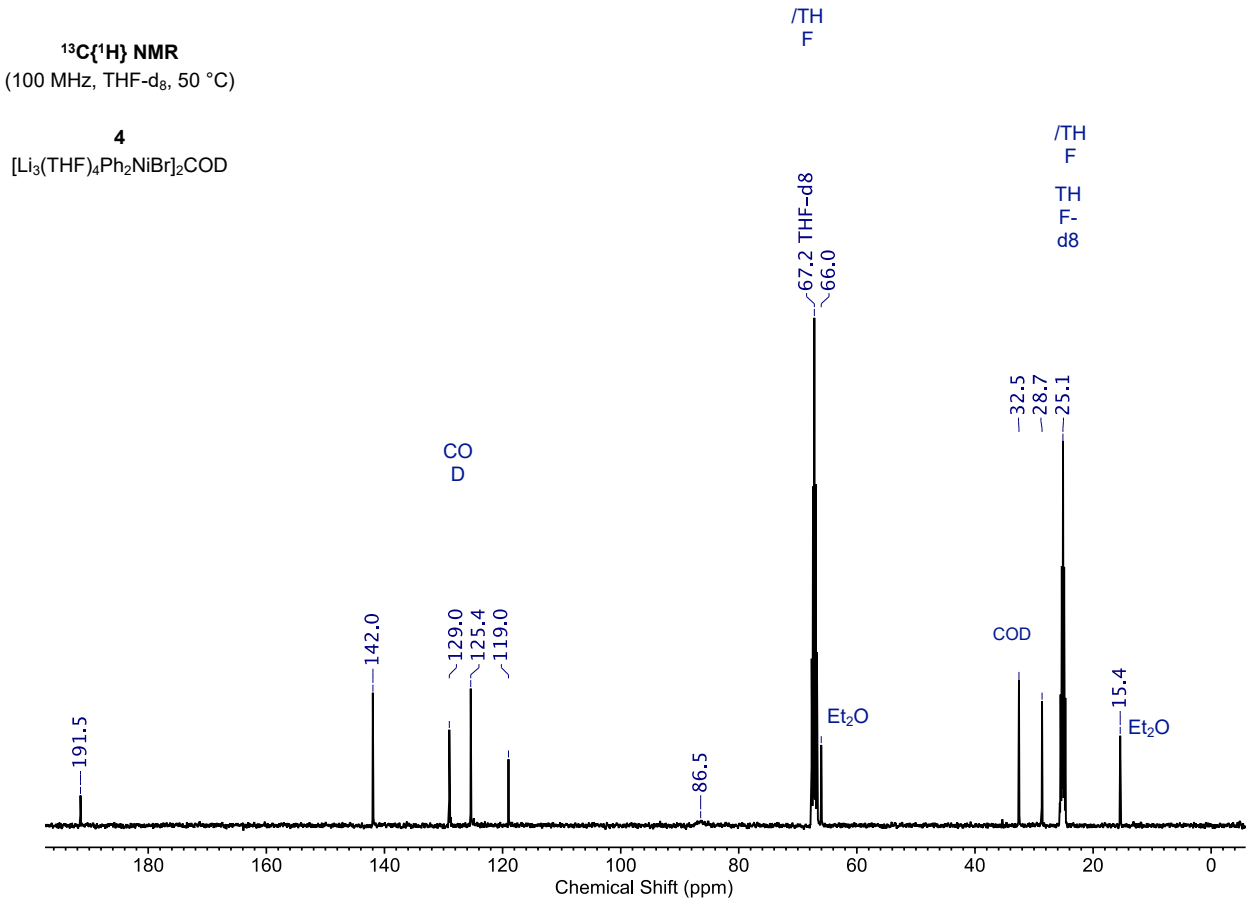

Spectrum S4: $^{13}C\{^{1}H\}$ NMR spectrum of **4** (*in situ* synthesis) in THF-d_8.

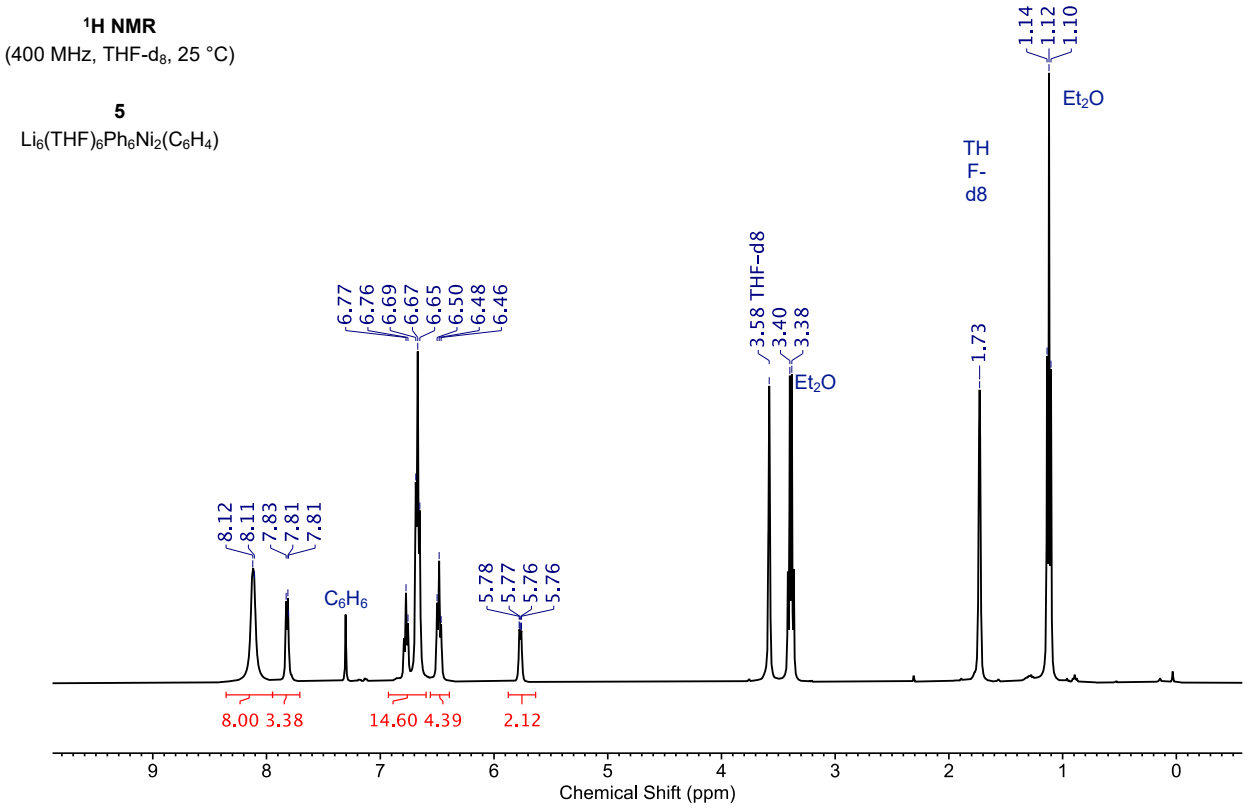

Spectrum S5: ^{1}H NMR spectrum of **5** in THF-d_8.

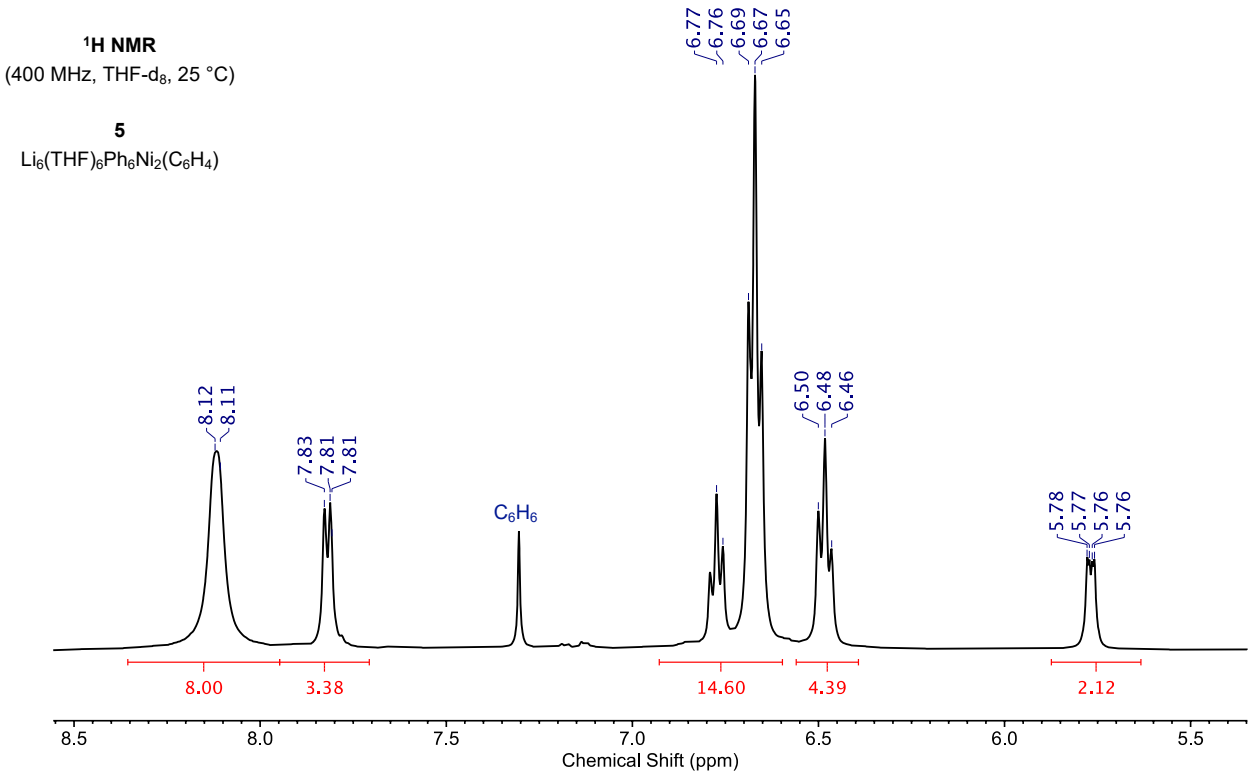

Spectrum S6: Expansion of ^{1}H NMR spectrum of **5** above.

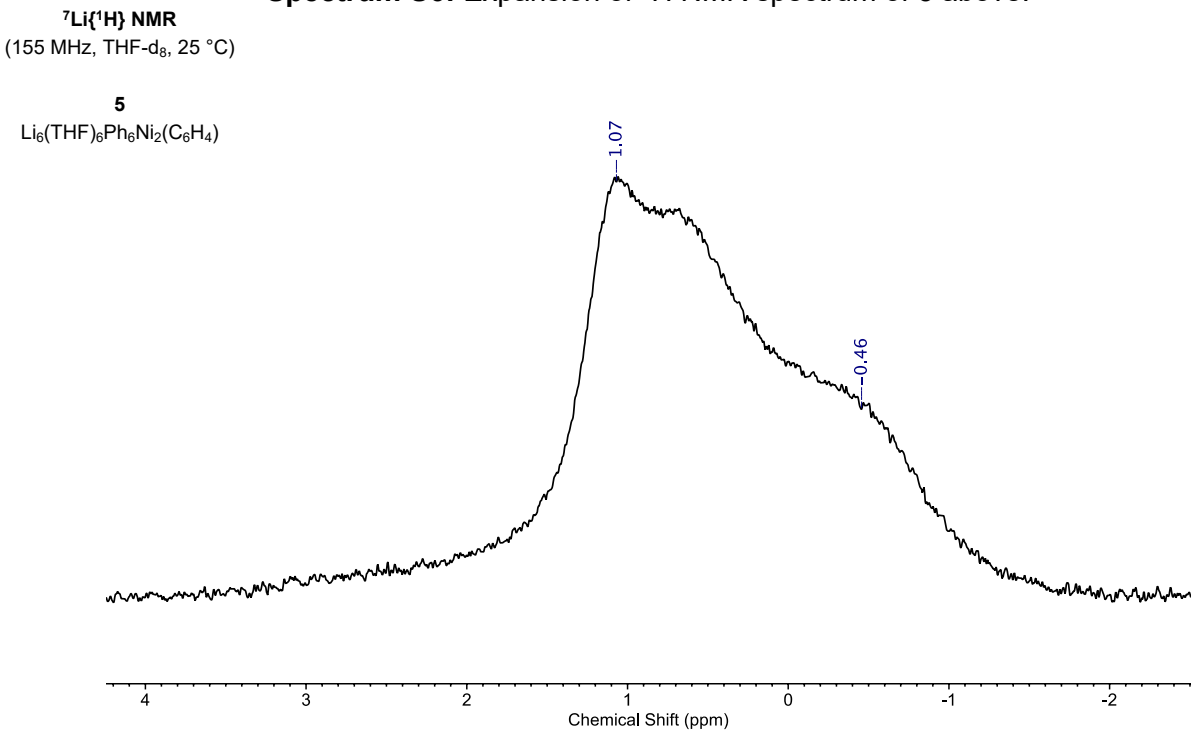

Spectrum S7: ^{7}Li{^{1}H} NMR spectrum of **5** in THF-d_8.

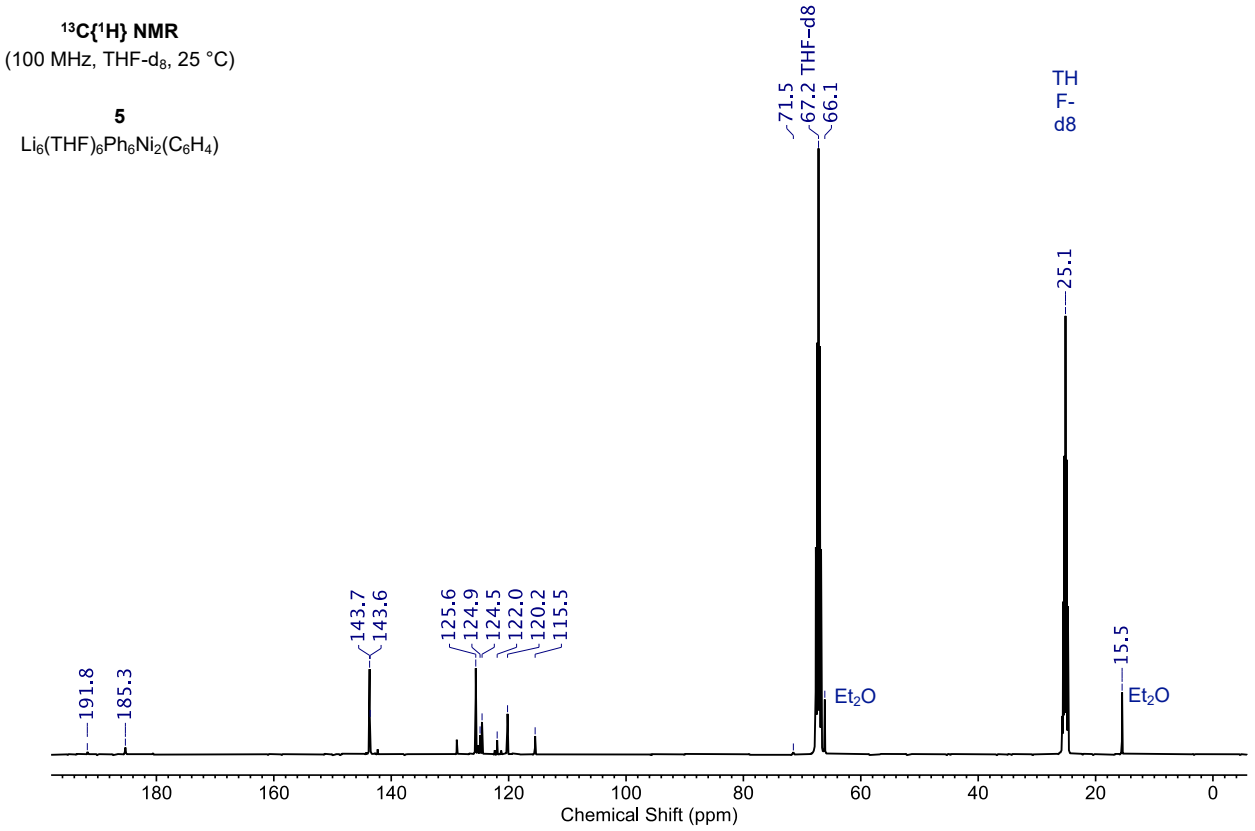

Spectrum S8: $^{13}C\{^1H\}$ NMR spectrum of **5** in THF-d_8.

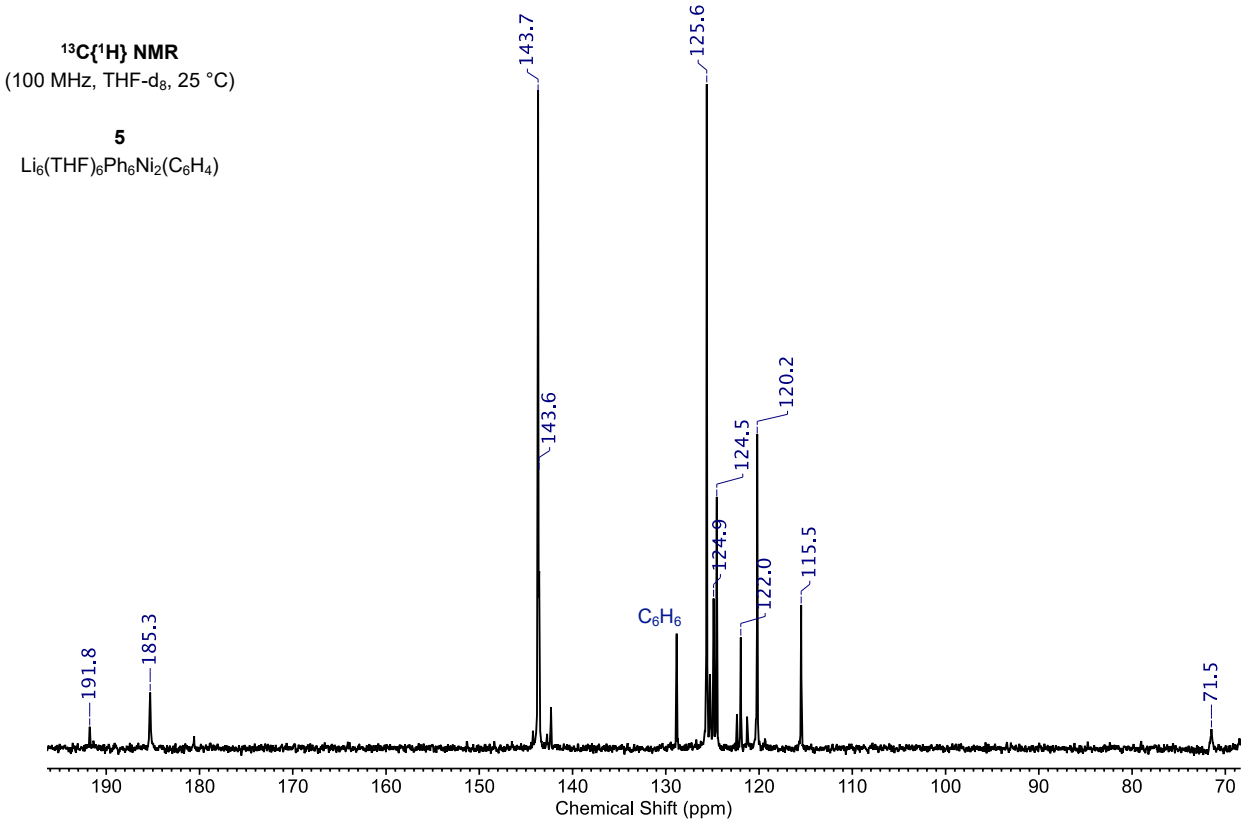

Spectrum S9: Expansion of $^{13}C\{^1H\}$ NMR spectrum of **5** shown above.

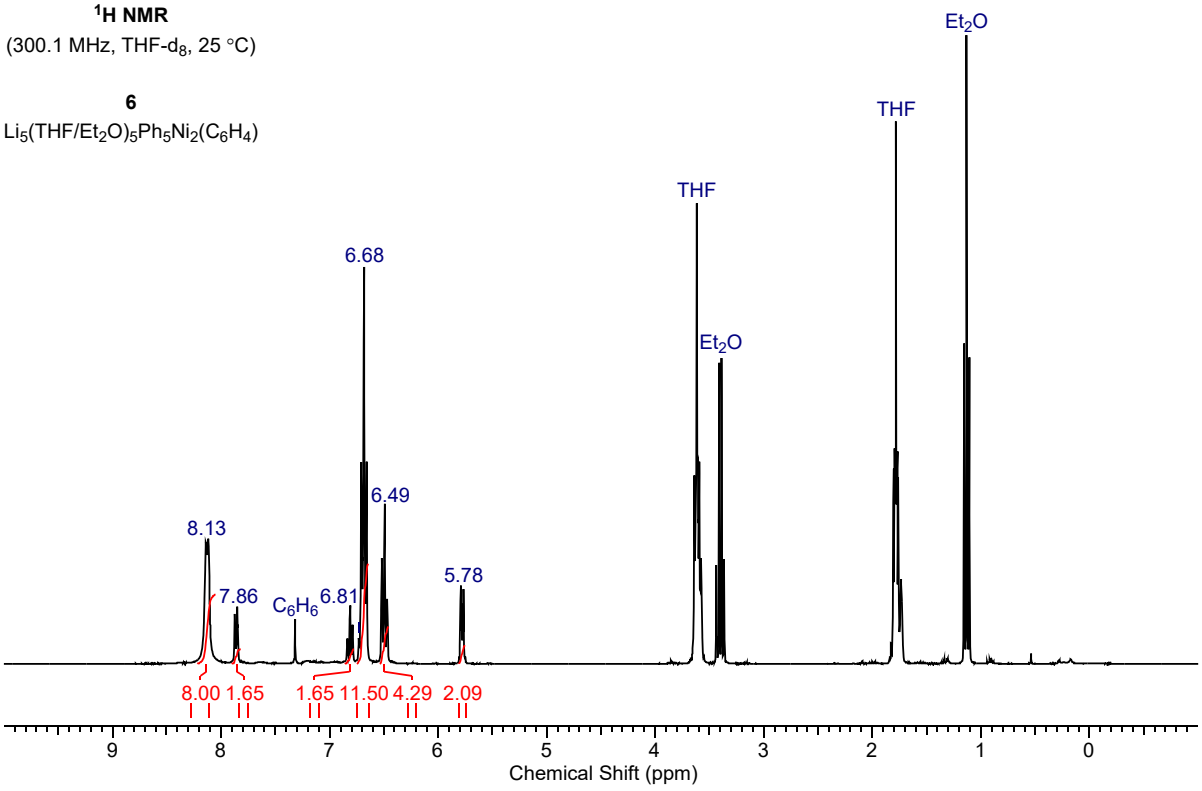

Spectrum S10: ^{1}H NMR spectrum of **6** in THF-d_8.

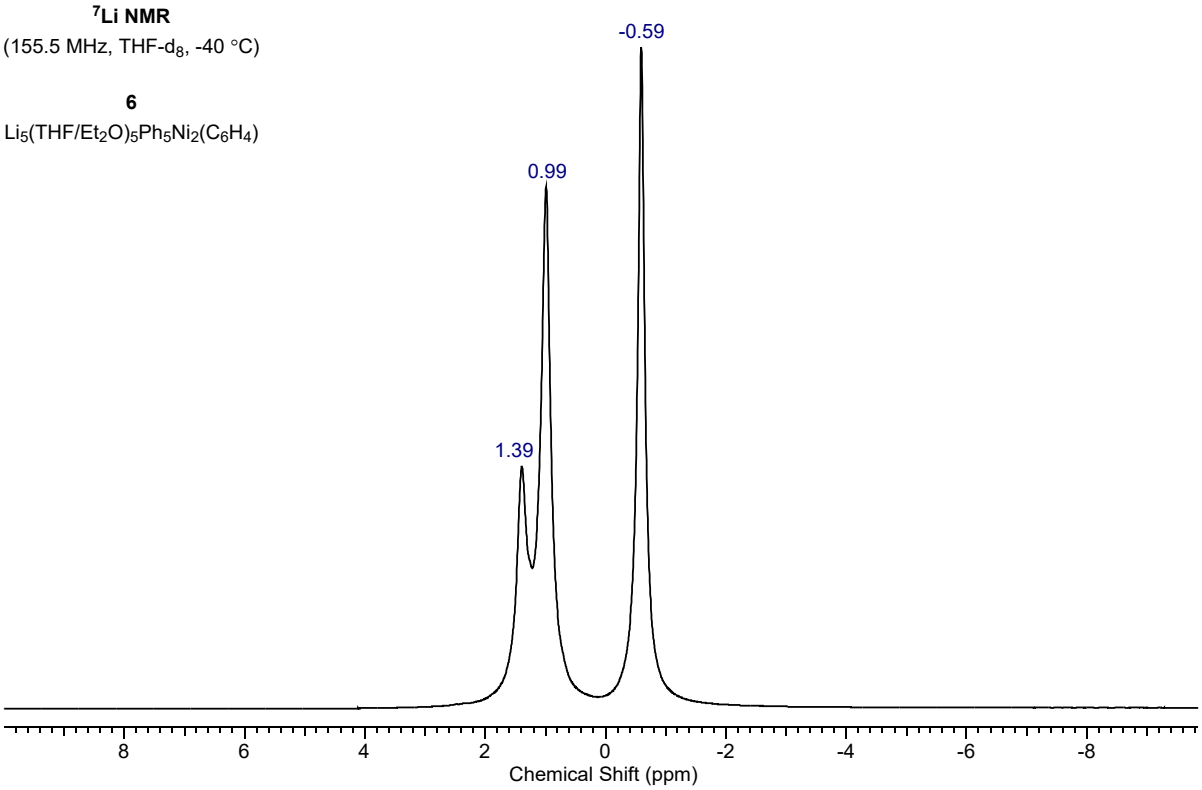

Spectrum S11: ^{7}Li NMR spectrum of **6** in THF-d_8.

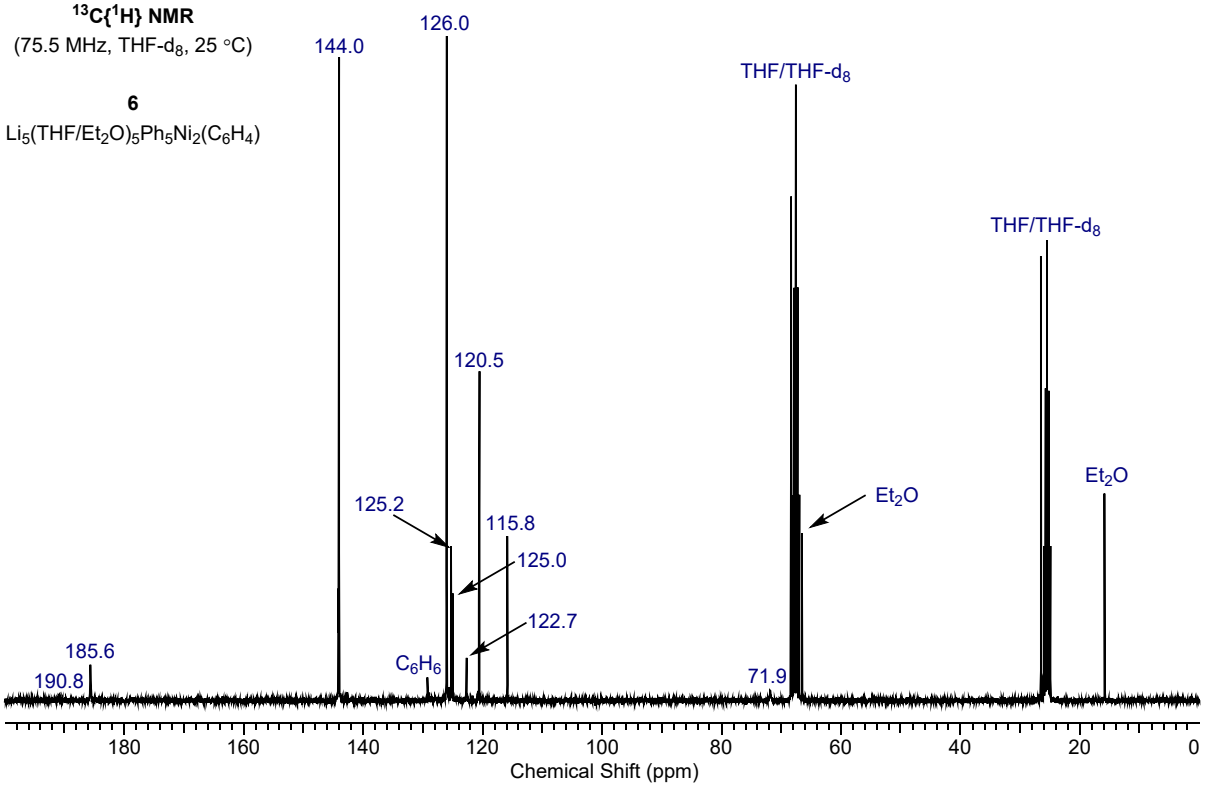

Spectrum S12: $^{13}C\{^{1}H\}$ NMR spectrum of **6** in THF-d_8.

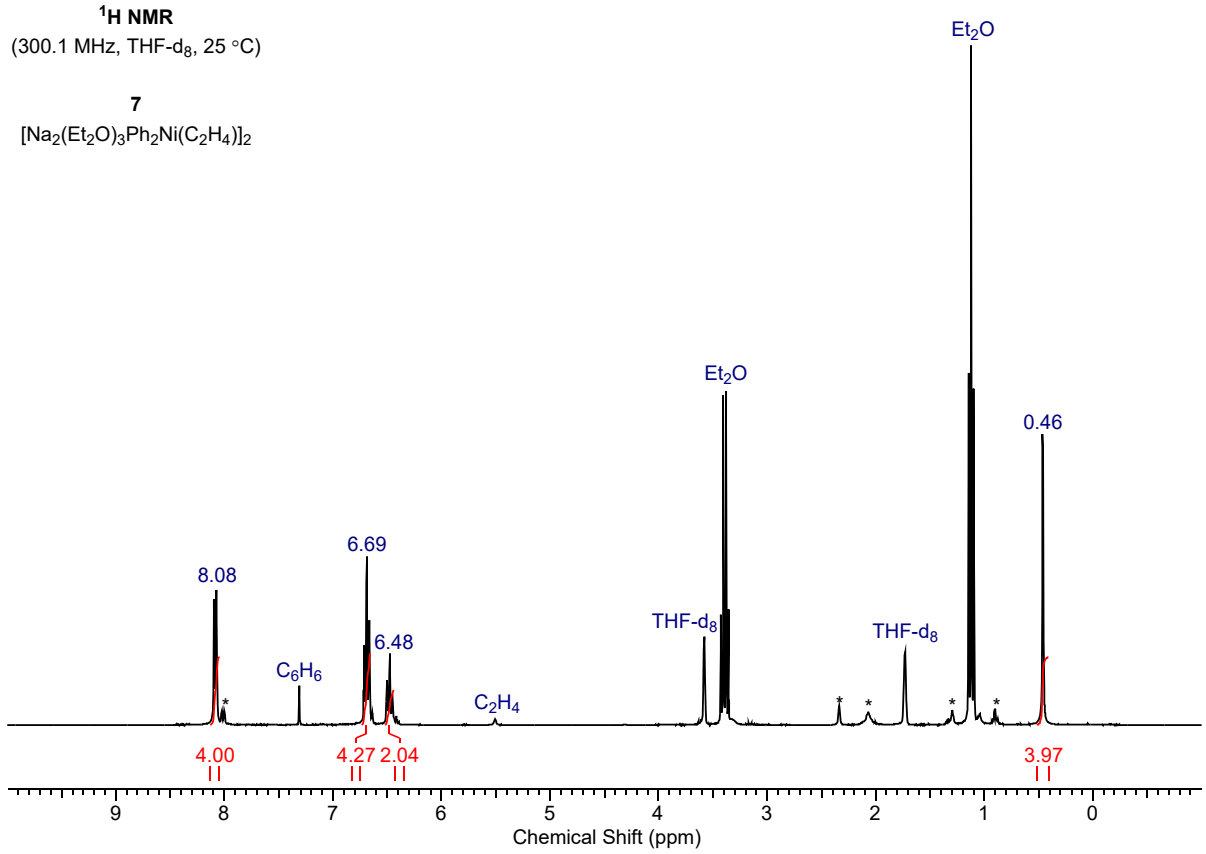

Spectrum S13: ^{1}H NMR spectrum of **7** in THF-d_8. * Trace impurities and residual hexane.

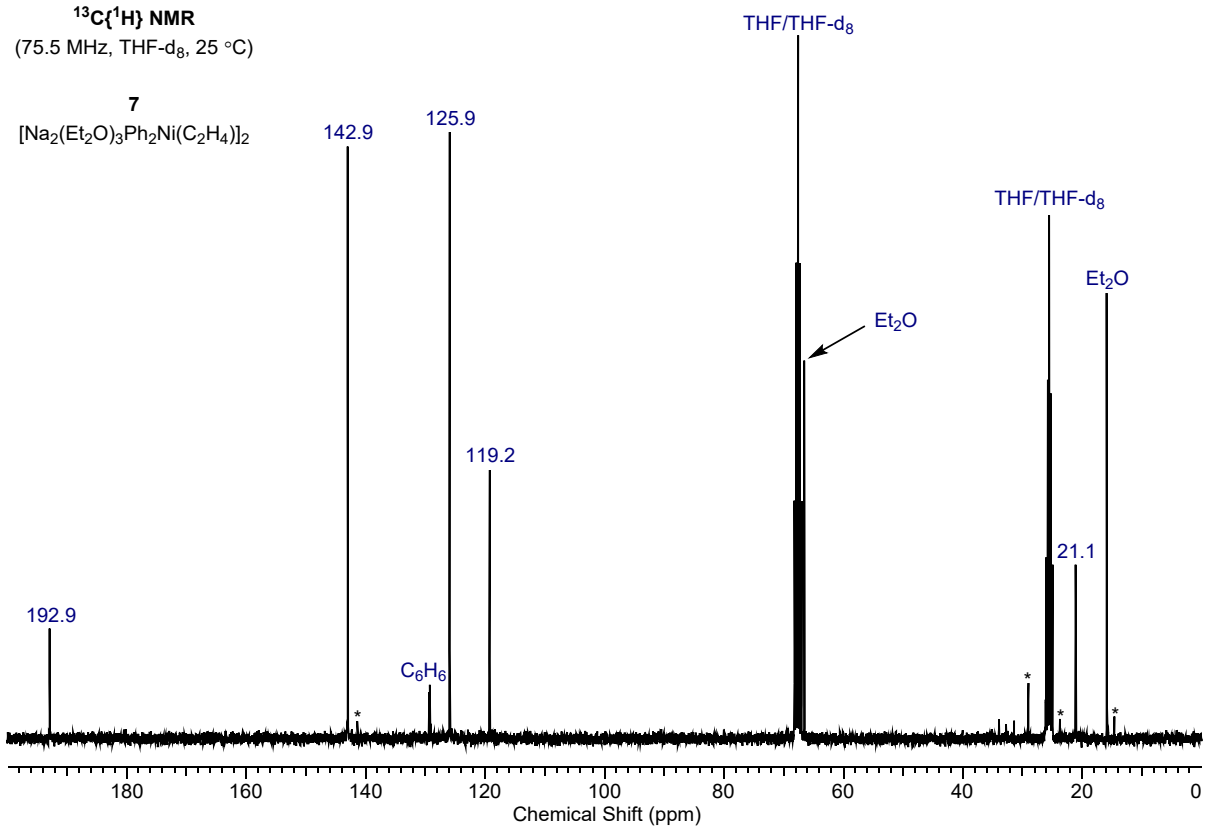

Spectrum S14: $^{13}C\{^1H\}$ NMR spectrum of **7** in THF-d_8. * Trace impurities and residual hexane.

Computational Details

Geometry optimizations of benzyne and **5** were performed using as starting geometry for **5** the major disorder component derived from the experimental X-ray diffraction results. Solvent molecules present in the crystal structure were not included in the optimization. Calculations were performed using Gaussian09[22] at B3LYP/def2-TZVP level of theory. Grimme-type empirical dispersion was included using the gd3bj method.[23] Frequency calculations were performed to guarantee the energy-optimized minimum was a global minimum on the potential energy surface by the absence of imaginary frequencies. The resulting geometry of **5** was compared to the geometry obtained via MN15//MN15L/def2SVP calculations to ensure that no artefacts would be produced when using both methods for the complementary bonding analysis.

Delocalization indices and bond paths within QTAIM were calculated from the optimized geometry using AIMALL with basin integration methods varying between Proaim and Promega (1st or 3rd order), automatically detected by the software (fine IAS Mesh).[24]

Grid files of electron density and ELI were calculated with the software dgrid.4-6.[25] Grid files for integration of electron density within the topological ELI basins had a point separation of 0.05 a.u. The

ELI basins were cropped at an outer electron-density isosurface of 0.001 a.u. so that they did not extend until infinity. Grid files for visualization were converted into the Gaussian cube file format using a point separation of 0.1 a.u. with dgrid. For compound **5**, the cube file obtained was then separated into individual cube files (one per basin) using the cuQCT software[26] and only the basins that corresponded to the benzyne-Ni moiety were selected to generate the plots using VMD.[27]

The NBO analyses were performed at the MN15/def2SVP level of theory on geometries fully optimized at the MN15L/def2SVP level. The calculations were carried out by using the NBO7 program, as implemented in Gaussian16 Rev. C.01. In addition to the NBO analysis of complex **5** discussed in the manuscript, the COD complex **2** was also analysed. As for **5**, the calculations predicted a closed-shell singlet ground state; open-shell states were unstable for both the singlet and triplet spin multiplicities. The deviation between the DFT geometry and crystal structure was also very small (RMSD = 0.003 Å, for all Ni–C distances). The NBO analysis showed that the $d_{Ni} \rightarrow \pi^*_{C=C}$ backdonation to the COD ligand is the strongest (SE = 158.9 kcal/mol), though it is much weaker than that to the benzyne ligand in **5** (SE = 474.1 kcal/mol). Furthermore, there are strong donor interactions from both the COD and PhLi ligands to the *s* orbital of Ni. Similar to **5**, donation from COD has a strong π component ($\pi_{C=C} \rightarrow s_{Ni}$; SE = 35.4 kcal/mol) and a weak σ component ($\sigma_{C=C} \rightarrow s_{Ni}$; SE = 3.7 kcal/mol). In contrast, the σ donation from the PhLi ligands is strong ($\sigma_{C\text{-}Li} \rightarrow s_{Ni}$; SE = 52.9 kcal/mol). This interaction is dominated by the *sp* orbital of the C atom and has a strength similar to that of the $sp_C \rightarrow s_{Ni}$ interaction in **5** (SE = 50.4 kcal/mol). Backdonation from the *d* orbitals of Ni to the σ*(C-Li) orbital of PhLi is weak (SE = 1.8 kcal/mol).

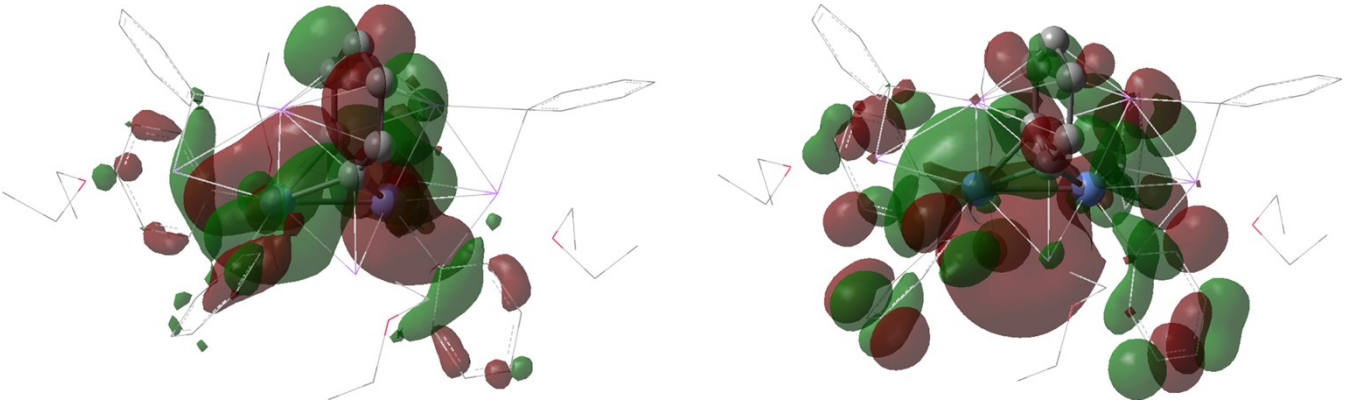

Figure S26: HOMO (left) and LUMO (right) molecular orbitals (isovalue = 0.02 a.u.) of full complex **5**. For clarity, H atoms were excluded. Representations: Ball-and-stick for the $Ni_2(\mu\text{-}C_6H_4)$ core and wireframe for the remainder.

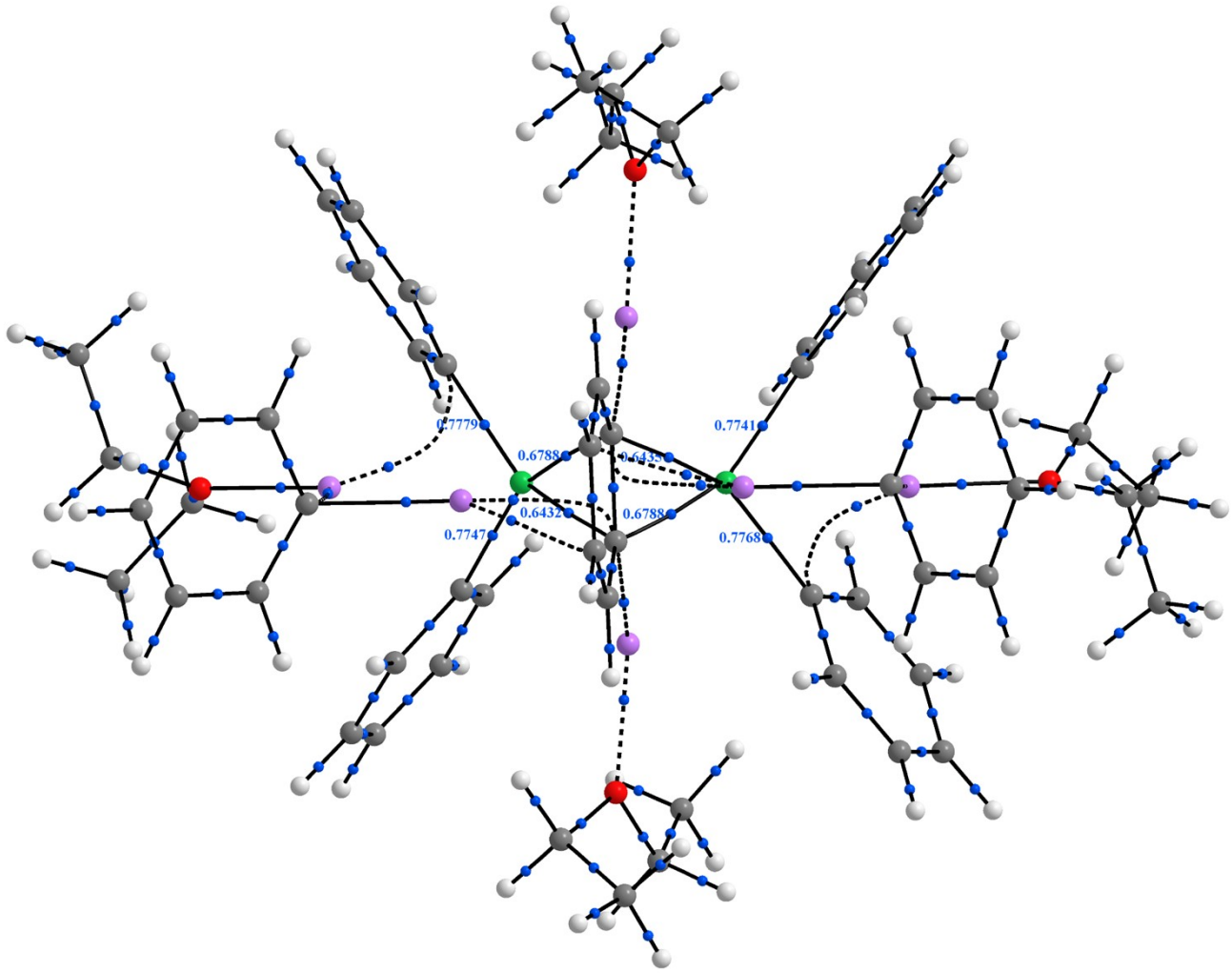

Figure S27: QTAIM molecular graph of complex **5**. Ni: green, Li: purple. Bond critical points: blue. Blue values are delocalization indices.

Raw output data from the NBO7 calculations (2nd order perturbation analysis) on full complex 5

Donor (L) NBO	Acceptor (NL) NBO	E(2)	E(NL)-E(L)	F(L,NL)
89. LP (3)Ni 1	266. LV (1)Ni 2	2.36	0.43	0.029
95. LP (4)Ni 2	265. LV (1)Ni 1	1.52	0.43	0.023
91. LP (5)Ni 1	278. BD*(2) C 6- C 7	452.08	0.03	0.111
96. LP (5)Ni 2	278. BD*(2) C 6- C 7	496.04	0.03	0.115
116. BD (2) C 6- C 7	265. LV (1)Ni 1	28.48	0.53	0.109
116. BD (2) C 6- C 7	266. LV (1)Ni 2	30.20	0.53	0.113
115. BD (1) C 6- C 7	265. LV (1)Ni 1	3.43	0.74	0.045
115. BD (1) C 6- C 7	266. LV (1)Ni 2	3.32	0.74	0.044
155. BD (1) C 27-Li142	266. LV (1)Ni 2	1.99	0.42	0.026

179. BD (1) C 45-Li144	265. LV (1)Ni 1	2.13	0.42	0.027
105. LP (1) C 11	265. LV (1)Ni 1	50.44	0.42	0.129
106. LP (1) C 12	266. LV (1)Ni 2	51.54	0.41	0.130
107. LP (1) C 13	266. LV (1)Ni 2	49.53	0.42	0.128
108. LP (1) C 14	265. LV (1)Ni 1	50.02	0.42	0.129

==========

For the E(2) stabilization energies, the article reports average values; *e.g.*, for d(Ni) → s(Ni), E(2) = 1.9 kcal/mol (NBOs 89 and 95 are lone-pair d(Ni) orbitals, whereas NBOs 265 and 266 are lone-vacancy s(Ni) orbitals).

References

S1 A. M. Borys, E. Hevia, *Angew. Chem. Int. Ed.* **2021**, *60*, 24659–24667.

S2 A. J. Roberts, A. R. Kennedy, R. McLellan, S. D. Robertson, E. Hevia, *Eur. J. Inorg. Chem.* **2016**, *2016*, 4752–4760.

S3 E. Negishi, D. R. Swanson, C. J. Rousset, *J. Org. Chem.* **1990**, *55*, 5406–5409.

S4 K. Lamm, M. Stollenz, M. Meier, H. Görls, D. Walther, *J. Organomet. Chem.* **2003**, *681*, 24–36.

S5 R. Taube, G. Honymus, *Angew. Chem. Int. Ed.* **1975**, *14*, 261–262.

S6 K. Jonas, *Angew. Chem. Int. Ed.* **1976**, *15*, 47.

S7 V. K. Jonas, C. Krüger, *Angew. Chem. Int. Ed.* **1980**, *19*, 520–537.

S8 R. Neufeld, D. Stalke, *Chem. Sci.* **2015**, *6*, 3354–3364.

S9 S. Bachmann, R. Neufeld, M. Dzemski, D. Stalke, *Chem. Eur. J.* **2016**, *22*, 8462–8465.

S10 S. Bachmann, B. Gernert, D. Stalke, *Chem. Commun.* **2016**, *52*, 12861–12864.

S11 L. Nattmann, S. Lutz, P. Ortsack, R. Goddard, J. Cornella, *J. Am. Chem. Soc.* **2018**, *140*, 13628–13633.

S12 G. Cahiez, O. Gager, F. Lecomte, *Chemtracts* **2010**, *23*, 9–11.

S13 T. Inatomi, Y. Fukahori, Y. Yamada, R. Ishikawa, S. Kanegawa, Y. Koga, K. Matsubara, *Catal. Sci. Technol.* **2019**, *9*, 1784–1793.

S14 A. Bismuto, P. Müller, P. Finkelstein, N. Trapp, G. Jeschke, B. Morandi, *J. Am. Chem. Soc.* **2021**, *143*, 10642–10648.

S15 K. Jonas, *Angew. Chem. Int. Ed.* **1973**, *12*, 997–998.

S16 C. Krüger, Y.-H. Tsay, *Angew. Chem. Int. Ed.* **1973**, *12*, 998–999.

S17 K. Jonas, D. J. Brauer, C. Krüger, P. J. Roberts, Y. H. Tsay, *J. Am. Chem. Soc.* **1976**, *98*, 74–81.

S18 Oxford-Diffraction, **2018**.

S19 G. M. Sheldrick, *Acta Cryst.* **2015**, *A71*, 3–8.

S20 G. M. Sheldrick, *Acta Cryst.* **2015**, *C71*, 3–8.

S21 O. V. Dolomanov, L. J. Bourhis, R. J. Gildea, J. A. K. Howard, H. Puschmann, *J. Appl. Crystallogr.* **2009**, *A42*, 339–341.

S22 M. J. Frisch, G. W. Trucks, H. B. Schlegel, G. E. Scuseria, M. A. Robb, J. R. Cheeseman, G. Scalmani, V. Barone, G. A. Petersson, H. Nakatsuji, X. Li, M. Caricato, A. V Marenich, J. Bloino, B. G. Janesko, R. Gomperts, B. Mennucci, H. P. Hratchian, J. V Ortiz, A. F. Izmaylov, J. L. Sonnenberg, D. Williams-Young, F. Ding, F. Lipparini, F. Egidi, J. Goings, B. Peng, A. Petrone, T. Henderson, D. Ranasinghe, V. G. Zakrzewski, J. Gao, N. Rega, G. Zheng, W. Liang, M. Hada, M. Ehara, K. Toyota, R. Fukuda, J. Hasegawa, M. Ishida, T. Nakajima, Y. Honda, O. Kitao, H. Nakai, T. Vreven, K. Throssell, J. A. Montgomery Jr., J. E. Peralta, F. Ogliaro, M. J. Bearpark, J. J. Heyd, E. N. Brothers, K. N. Kudin, V. N. Staroverov, T. A. Keith, R. Kobayashi, J. Normand, K. Raghavachari, A. P. Rendell, J. C. Burant, S. S. Iyengar, J. Tomasi, M. Cossi, J. M. Millam, M. Klene, C. Adamo, R. Cammi, J. W. Ochterski, R. L. Martin, K. Morokuma, O. Farkas, J. B. Foresman, D. J. Fox, *Gaussian 09, Revision D.01*, Gaussian, Inc., Wallingford CT, **2016**.

S23 S. Grimme, S. Ehrlich, L. Goerigk, *J. Comput. Chem.* **2011**, *32*, 1456–1465.

S24 T. A. Keith, *AIMAll (Version 19.02. 13)*, TK Gristmill Software, Overland Park KS, USA, **2019**.

S25 M. Kohout, *DGrid, Version 4.6*, Radebeul, **2011**.

S26 F. Kleemiss, E. K. Wieduwilt, E. Hupf, M. W. Shi, S. G. Stewart, D. Jayatilaka, M. J. Turner, K. Sugimoto, E. Nishibori, T. Schirmeister, T. C. Schmidt, B. Engels, S. Grabowsky, *Chem. Eur. J.* **2021**, *27*, 3407–3419.

S27 W. Humphrey, A. Dalke, K. Schulten, *J. Mol. Graph.* **1996**, *14*, 33–38.